University of California

Los Angeles

# A Mathematical Model of Cardiac Action Potential: Application to Wave Propagation

A dissertation submitted in partial satisfaction

of the requirements for the degree

Doctor of Philosophy in Computer Science

by

**Mikhail Karpoukhin**

1996

The dissertation of Mikhail Karpoukhin is approved.

James N. Weiss

Jacques J. Vidal

Jack W. Carlyle

Boris Y. Kogan, Committee Co-Chair

Walter J. Karplus, Committee Co-Chair

University of California, Los Angeles

1996

*To my wise teachers...*

## Table of Contents

## List of Figures

# ACKNOWLEDGMENTS

I owe many thanks:

To my academic advisor Prof. Boris Kogan for his inspiration and ideas. It was through many hours of work, discussions and arguments with Prof. Kogan that I learned what real science is about. He has taught me that one can succeed in science only through total dedication to it. His outstanding achievements in science and life are a perfect example of that. I am thankful to Prof. Kogan for sharing his vast knowledge and experience, and I am proud to be one of his students.

To Prof. Walter Karplus for his guidance, diplomacy and wisdom.

To Prof. James Weiss and Prof. Alan Garfinkel for their deep interest in this work and very helpful discussions.

To the members of my committee, Prof. Jacques Vidal and Prof. Jack Carlyle, for their kind words, suggestions, and cooperation.

To Verra Morgan for introducing me to Prof. Kogan and for invaluable help in academic affairs.

To Brian Billett for teaching me how to do the Connection Machine simulations, and for sharing the fun of doing a poster.

To Rebecca Hwa, Paula Dennehy and Boris Shimanovsky for their help with simulations.

To Michael Harreld for being around when I needed company, advice, encouragement, help, and for setting up the high pace in our competition "who is the first to graduate".

To Bob Tisdale for being my informal mentor, teaching me UNIX, and providing all necessary hardware.

To my other fellow graduate students and friends at UCLA, Simon Shpilfoygel (for endless stream of e-mails and practical jokes), Igor Roizen (for finding errors in my programs), Eugene Chudin (for fun with chess).

To the big Kashper family. Without their love, help and support this work would not have been possible.

To Nadya Landau and Tatiana Fedorova for providing the perfect environment for work at home.

To my parents for their love and support of all my vital decisions.

To IEEE for the permission to reprint in chapter 3 portions of the paper: Mikhail G. Karpoukhin, Boris Y. Kogan, and Walter J. Karplus. "The Application of a Massively Parallel Computer to the Simulation of Electrical Wave Propagation Phenomena in the Heart Muscle Using Simplified Models." In *Proceedings of the Twenty-Eighth Annual Hawaii International Conference on System Sciences. Biotechnology Computing*, volume 5, pp. 112–122. IEEE Computer Society Press, 1995. Copyright ©1995 IEEE.

To Computational Mechanics Publications for the permission to reprint in chapter 4 portions of the paper: B.Y. Kogan, W.J. Karplus, and M. Karpoukhin. "The Third-Order Action Potential Model for Computer Simulation of Electrical Wave Propagation in Cardiac Tissue." In *Computer Simulations in Biomedicine*, editors H. Power and R.T. Hart. Computational Mechanics Publications, Southampton Boston, 1995. Copyright ©1995 Computational Mechanics Publications.

This work was supported in part by the NASA/Dryden Research Center under

Grant NCC 2-374, and NSF under Grant BBS 87-14206 for research in the use of massive parallelism for system simulation. It was also supported by the NIH Grant SCOR in Sudden Cardiac Death P50 HL52319 for research in the computer simulation of heart arrhythmia.

# Vita

| | |
|---|---|
| 1965 | Born, Saint Petersburg, Russia. |
| 1985–1988 | Research Assistant, Electrical Engineering Institute, Saint Petersburg, Russia. |
| 1988 | Degree of Electrical Engineer, Electrical Engineering Institute, Saint Petersburg, Russia. |
| 1989–1991 | Researcher, Electrical Engineering Institute, Saint Petersburg, Russia. |
| 1992–1993 | Research Assistant, Department of Mechanical, Aerospace and Nuclear Engineering, UCLA, Los Angeles, California. |
| 1993–present | Research Assistant, Computer Science Department, UCLA, Los Angeles, California. |
| 1994 | M.S. (Computer Science), Computer Science Department, UCLA, Los Angeles, California. |

## Publications and Presentations

B.S. Billett, M. Karpoukhin, and B.Y. Kogan. "Computer Simulation of Excitation Wave Front Transients." *Research Review*, Computer Science Department, UCLA, March 1993.

Mikhail G. Karpoukhin, Boris Y. Kogan, and Walter J. Karplus. "The Application of a Massively Parallel Computer to the Simulation of Electrical Wave Propagation Phenomena in the Heart Muscle Using Simplified Models." In *Proceedings of the Twenty-Eighth Annual Hawaii International Conference on System Sciences. Biotechnology Computing*, volume 5, pp. 112–122. IEEE Computer Society Press, 1995.

B.Y. Kogan, W.J. Karplus, B.S. Billett, and M. Karpoukhin. "On the Applicability of the Ashour–Hanna Numerical Algorithm for the Investigation of Diffusion–Reaction Equations." Technical Report 910076, Computer Science Department, UCLA, November 1991.

B.Y. Kogan, W.J. Karplus, B.S. Billett, and M. Karpoukhin. "Excitation Wave Front Transients: A Computer Simulation Study." In *Proceedings of the 15th Annual International Conference of the IEEE Engineering In Medicine and Biology Society*, pp. 28–31. San Diego, CA, October 1993.

B.Y. Kogan, W.J. Karplus, and M.G. Karpoukhin. "The Van Capelle and Durrer Model of Cardiac Action Potential Generation and 2D Propagation: Modifica-

tions and Application to Spiral Wave Propagation – Part I." Technical Report 940002, Computer Science Department, UCLA, January 1994.

B.Y. Kogan, W.J. Karplus, and M. Karpoukhin. "The Third-Order Action Potential Model for Computer Simulation of Electrical Wave Propagation in Cardiac Tissue." In *Computer Simulations in Biomedicine*, editors H. Power and R.T. Hart. Computational Mechanics Publications, Southampton Boston, 1995.

B.Y. Kogan, W.J. Karplus, and M. Karpoukhin. "The Van Capelle and Durrer Model of Cardiac Action Potential Generation and 2D Propagation: Modifications and Application to Spiral Wave Propagation." In *Simulation in the Medical Sciences conference. Proceedings of the 1996 Western Multiconference*, editors James G. Anderson and Meyer Katzper, pp. 106-112. The Society for Computer Simulation, January 1996.

Abstract of the Dissertation

# A Mathematical Model of Cardiac Action Potential: Application to Wave Propagation

by


**Mikhail Karpoukhin**

Doctor of Philosophy in Computer Science

University of California, Los Angeles, 1996

Professor Walter J. Karplus, Co-Chair

Professor Boris Y. Kogan, Co-Chair



Heart fibrillation, the main reason for sudden cardiac death, can be studied on the computer using mathematical models of action potential propagation. Full physiological models are difficult to use due to their complexity. Existing simplified models suffer from a number of drawbacks. In this research existing simplified models are studied to find out their advantages and disadvantages. This is accomplished by comparative analysis, using a developed common approach, of the three most popular simplified models: FitzHugh-Nagumo, Van Capelle and Karma. As a result, a new method of simplified model synthesis is developed, and a new third-order model is proposed which correctly reproduces the shape of action potential and the cell recovery processes. The third-order model is based on the Luo–Rudy I action potential model. The model uses the Ashour-Hanna numerical algorithm for integration, tables of the non-linear functions for speed up and a table of action potential duration restitution for flexibility. The generation

of function and action potential duration restitution tables and the measurement of the action potential parameters are performed automatically using the proposed algorithm. The interactive graphical user interface of the simulation program allows the researcher to intervene in the simulation process.

The study of one-dimensional action potential propagation in a ring of cells using this model uncovered a double-valued shape of the dynamic action potential duration restitution curve. The quasi-periodic instability in action potential propagation was studied for different ring lengths and for different kinds of static action potential duration restitution curves. The distribution of the action potential duration along the ring during the quasi-periodic instability is periodic with a period less than two ring lengths. The simulation of two-dimensional propagation showed the breakup of non-stationary spiral waves, which is different from that obtained using other simplified models. It is shown that the presence of maximum speed of depolarization restitution changes the character of one- and two-dimensional propagation. In particular, in the two-dimensional case it leads to the irregular structure of multiple spiral waves.

Finally, the contributions are outlined, and directions for future study are mentioned.

# CHAPTER 1

# Introduction

## 1.1 Overview of the Problem

It is a well established fact that the main reason for sudden cardiac death is heart fibrillation. The mechanisms of cardiac fibrillation appearance are unknown, especially in the originally healthy heart. The study of this phenomenon in vivo represents great difficulties due to the complex interaction of different processes which determine heart functions, difficulty in measuring the action potential (AP) propagation inside the heart muscle, and the inability to change independently different characteristics and parameters which are responsible for the excitation wave propagation in the heart. Computer simulation in combination with the physiological studies represents one of the instruments for solving this important problem.

Computer simulation requires the mathematical model of AP generation and propagation. Progress in cell membrane theory and clamp experiment techniques achieved in the past two decades has led to the development of sophisticated mathematical models of cardiac cells. They describe the electrophysiological processes in isolated cardiac cells with comparatively high accuracy and in great detail. These models are very useful for the simulation of detailed cell mechanisms, but appear to be too complicated for the simulation of AP propagation in 2D and 3D cardiac tissue. Even modern massively-parallel and supercomputers are not fast enough to permit interactive computer experiments using these models.

A number of successful attempts have been made to provide simplified models. These models can be divided into three main groups. Models of the first group are based on reducing the sophisticated mathematical description of the ion models to two first-order differential equations using singular perturbation theory [Tik52]. Krinsky was one of the first researchers who applied this approach to the Hodgkin-Huxley nerve axon model and the Noble cardiac Purkinje fiber model [KK73]. The well known and widely-used Van Capelle – Durrer (VC-D) [VD80] and Karma [Kar93] models belong to this group. The first was proposed for ischemic heart muscles with low depolarization rates and low conduction velocities and was intended for implementation on a PC. The second is based on the experimental data used in the Noble model for Purkinje fiber with some small changes. Both models use quite different analytical expressions for the approximation of the experimental data.

Models of the second group use the hypothesis of mutual dependence of sodium activation and inactivation processes proposed by R. Hoyt [Hoy68]. These principles were realized in the simplified model by Gulko [GP70].

Models of the third group are not ionic models in the common sense of the term. Among them, the FitzHugh-Nagumo (FH-N) model [Fit69], based on the principles of the Van der Pol relaxation generator [VV28], is the most widely used. Many computer simulation studies of 2D and 3D tissue were performed on different modifications of this model (see, for example, [KKB91b, PCP81, PDS93]).

All of these models are based on old experimental data and provide only qualitative results. They do not reproduce the cell recovery processes and the shape of AP properly. Now, more detailed physiological data are available, which makes it possible to revise the approach to the synthesis of the simplified models.

In this research, existing simplified models are analyzed and compared, and a new approach to the synthesis of simplified models is proposed. This approach is based on the idea that generation and propagation of AP can be considered as separate problems, which can be solved using different models of AP.

## 1.2 Importance and Implications

Every day, sudden cardiac death, or the unexpected onset of a fatal arrhythmia, kills more than a thousand people in the United Sates alone. The majority of these cases begin as ventricular tachycardia, which degenerates to fibrillation, where the heart can no longer pump blood. Understanding this abrupt transition from a spatially organized rhythm to seemingly random and disorganized behavior is a challenging task.

Since the electrical behavior of the heart changes rapidly in time and space, measurement and investigation of intact hearts is difficult. Computer simulation provides an avenue for studying this problem and its subtleties in depth. In addition to examining the normal electrical activity in the heart, computer simulation allows us to study the abnormalities in AP propagation and the effect of drugs on it. All of this makes the computer simulation an invaluable tool for physiologists working on heart problems.

The results of this scientific effort combined with the results of physiological experiments have direct implications to the understanding and treatment of cardiac arrhythmias and fibrillation:

- The recovery dynamics of an action potential, which can be altered by drugs, can facilitate or inhibit reentrant arrhythmia in the myocardium;
- Specific knowledge of propagation dynamics and nature can lead to the development of more advanced methods of arrhythmia treatment and fibrillation control.

Successfully expanding the computer implementation, and achieving new scientific results also has implications to engineering and non-linear science:

- Utilizing interactive simulation and visualization of phenomena in excitable media can facilitate human insight into those systems;
- Our specific implementation on massively-parallel and serial computers, and interactive visualization and measurement is a successful tool for investigating excitable media, particularly cardiac tissue.

## 1.3 Scope of Investigation

The latest full ionic models of AP provide a very precise description of the cell AP. However, due to their complexity, they cannot be used to study AP propagation interactively even on supercomputers. Therefore, for the purpose of studying the AP propagation we have to consider simplified models. A number of simplified models were developed, which are based on different principles. The first step would be to analyze and compare these models to see which of them are more suitable for the simulation of AP propagation. All of these models provide only qualitative results since they are based on the obsolete clamp experiment data. To improve the quality of the result, a new simplified model has to be created which employs the latest physiological data.

This model, then, can be applied to the simulation of 1D and 2D AP propagation. The 1D simulations will allow us to verify the new model for AP propagation and to study the shape of the propagating AP. In addition, the study of 1D propagation in a ring of cells will reveal the reasons for instability and action potential duration (APD) oscillations observed earlier [CGK93]. The simulation of 2D propagation will provide a better understanding of the non-stationary spiral wave propagation and its breakup.

The problem of AP simulation belongs to the class of stiff problems. Therefore, special care has to be taken in the selection of a numerical algorithm and the optimization of a simulation program for computational time. Analysis tools, including the measurement of AP parameters, velocity and distribution in space, and the visualization of these, are crucial elements for understanding the results of propagation simulation. Developing and utilizing these tools in the course of the investigation is in itself an important result.

The investigation can be broken down into the following components:

1. **The overview and analysis of the existing simplified models**

   The overview of the models, presented in chapter 2, shows that among the simplified models the more advantageous for propagation studies are simplified ionic models. These models are very different and, in order to select a proper model, the detailed analysis of existing simplified models was carried out in chapter 3. For this purpose a new general approach was developed which is based on the analysis of inward and outward currents on the phase plane. It was found that all existing second-order models suffer from some drawbacks and can not produce the correct quantitative results.

2. **The synthesis of the third-order simplified model**

   A detailed research was undertaken to determine what causes the drawbacks in simplified models. At the same time, a new approach to the synthesis of simplified models was proposed. This approach is based on the separation of all membrane currents into two groups: currents involved in the depolarization phase of AP and currents involved in the repolarization phase. As a result of this research, the method of synthesis of the third-order mathematical models was formulated in chapter 4. The synthesized third-order simplified model is based on the Luo – Rudy I (LR) [LR91] full ionic model and consists of three first-order differential equations and seven non-linear functions.

3. **One-dimensional AP propagation**

   The results of simulation of 1D AP propagation in the ring are presented in chapter 5. The simulation allowed to further verify the new model and adjust its parameters to reflect the realistic speed of propagation. The ring simulations were used to study the shape of the propagating AP and the dependence of the propagation stability on the different APD restitution characteristics and different lengths of the ring.

4. **AP propagation in 2D tissue**

   The investigation of the 2D propagation using the third-order model is done in chapter 6. This includes the propagation of the non-stationary spiral wave and its spontaneous breakup. The importance of this investigation is connected to the fact that the spiral wave can be considered a prototype of the stationary arrhythmia and the spontaneous breakup of the non-stationary spiral wave a prototype of heart fibrillation.

# CHAPTER 2

# Overview of the Models of Cardiac AP

## 2.1 Full Mathematical Models

### 2.1.1 Noble model

Hodgkin and Huxley [HH52] were the first to develop the ionic model for AP generation and propagation in nerve fiber. This model was modified by Noble [Nob62] for heart Purkinje fiber. The Purkinje fiber has the ability for spontaneous AP generation. By changing the value of constant sodium conductivity the Noble model was adjusted for simulation of AP in working myocardium. This model takes into account only two ionic currents: sodium inward current and potassium outward current. The latter consists of two components: time-dependent and time-independent. The time-dependent component of potassium current is controlled by the gate variable $n$.

### 2.1.2 Luo and Rudy model

The development of the clamp experiment technology (transfer from patch of cells to a single cell clamp experiment) led to the synthesis of a number of new more sophisticated models: Noble [DN85, MNT75], Beeler-Reuter [BR77], Ebijara-Johnson [EJ80] and Luo-Rudy [LR91, LR94]. The Luo-Rudy model is the eight-order model with seventeen non-linear functions. The currents in this model are controlled by six gate variables. The investigation of the LR model showed that three out of six gate variables do not return to their initial values during the duration of AP. The same is true for the second version of the LR model.

The changes of the gate variables which occur after the cell goes out of excitation reflect the recovery processes in the cell. This is very important in the case of repeatable excitation of the cell which occurs in wave propagation along the ring and in spiral wave in 2D and 3D excitable tissue. For small diastolic intervals these recovery processes cause the decrease of the $(dE/dt)_{max}$, while the decrease of APD is observed during not only small, but relatively large diastolic intervals.

If we represent the myocardium as a 2D uniform lattice each node of which consists of a patch of cells, then the amount of nodes in the lattice necessary for the spiral wave formation has to be greater than 1000 (see Moe [MRA64]). So, using the eight-order LR model we have to solve more then 8000 nonlinear ordinary differential equations simultaneously. The power of today's supercomputers is not enough to allow the interactive simulation of such problem. That is why simultaneous to the development of full physiological models, a lot of efforts were made to develop the simplified models.

## 2.2 Simplified Mathematical Models

Historically, three different approaches were proposed to the simplification of the cardiac cell models: the phenomenological approach, order reduction, and physical analogy. The taxonomy of simplified models is presented in Fig. 2.1.

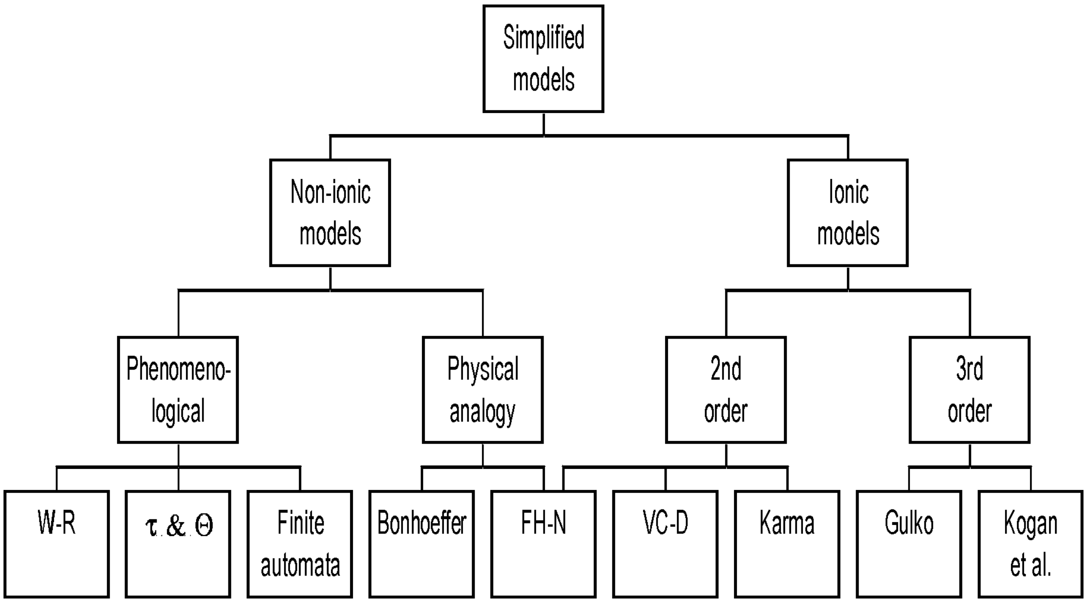


Figure 2.1: The taxonomy of simplified models.

### 2.2.1 Phenomenological approach

This approach is based on the axiomatic postulation of a limited number of external characteristics of the excitation wave propagation process. The phenomenological approach was first presented in rigorous and finished form by Wiener and Rosenblueth (WR) [WR46]. Here, an excitable medium is viewed as a collection of interacting excitable elements, and it is postulated that each of these elements can be found in one of the three states: resting, excited or refractory. Elements in the rest state can be excited if at least one element connected with them is excited. An element can not be excited if it is in the refractory state. Excitation is transmitted from certain elements to other neighboring ones only by leading front of the excitation wave. It is postulated that the velocity of propagation $\Theta$ and duration of the refractory period $R$ are constant.

The evolution of phenomenological models after the seminal work [WR46] went along the path of taking into account additional properties of the medium observed experimentally. For example, in the model proposed by Gelfand and Tsetlin [GT60], in addition to the WR postulates, the possibility of spontaneous activity for each point of the medium and the dependence of the propagation velocity on the time lapsed from the instant of its latest excitation were also taken into account. Rosenblueth proposed the $\tau$-model of an excitable element. The excitable element in this model is able to transmit excitation to neighbors for time $\tau$ after excitation, where $\tau$ is smaller than the refractory period. Krinsky proposed a $\Theta$-model [Kri71], which is based on the delay $\Theta$ in the appearance of AP in response to the repeated excitation in the interval $T$ between a pair of excitation pulses. Moe [MRA64] added to the phenomenological model the dependence of the refractory period on the length $T$ of the preceding excitation cycle and showed the possibility of the spiral wave circulation in 2D medium in the absence of anatomical obstacles. He also introduced the definition of the critical heart mass for fibrillation. Some authors proposed to use a finite automata as a phenomenological model. Tyson [TK88] observed a phenomenon qualitatively similar to spiral wave propagation in the network of such automatas.

From the above comments it is obvious that at first glance minor modifications of the phenomenological model properties lead to the emergence of qualitatively new ideas of the mechanisms of wave propagation. However, since these models don't take into account biological properties of the cell, they give substantial qualitative and quantitative differences in results when compared to the physiological models.

### 2.2.2 Order reduction

The reduction of the order of ODEs, which describe the full mathematical model, is possible by taking into consideration that in AP generation there are two main processes (depolarization and repolarization) which differ significantly in speed. For instance, in the Noble model the time constants which characterize the depolarization processes have the following numerical values: $\tau_m \approx 10^{-4}s$, $\tau_h \approx 5 \times 10^{-3}s$ while $\tau_n \approx 10^{-1}s$. This allows for the separation of all currents into the depolarization and repolarization groups which can be described by different ODEs. Using singular perturbation theory it was shown by Krinsky et al. [IKS78] that it is possible to reduce this system to the second order one. In [KK73] Krinsky demonstrates how to reduce Noble's fourth order differential equation for Purkinje fiber to the second order equation.

The second order simplified models obtained using this approach are unable to reproduce the overshoot preceding the plateau phase, which is typical for the heart muscle AP, and have a substantially decreased leading-front steepness due to the replacement of the fast changing gate variables with their steady state values. However, they allow us to decrease the computation time significantly and open possibilities for phase plane analysis.

### 2.2.3 The use of physical analogy

This approach is based on the analogy between phenomena of different physical nature. For example, Ostwald [Ost00] in 1900 noticed that the propagation of oxidation reaction after the application of electrical stimulus to iron wire immersed in a strong solution of nitric acid resembled the generation and propagation of action potential along the nerve fiber. Bonhoeffer [Bon59] derived the full mathematical description of this electro-chemical phenomenon which appears to be similar to that of the electrical wave propagation in nerve fiber. Van der Pol [VV28] put into correspondence the relaxation oscillation generators connected in series and a heart bit generation system. The Van der Pol relaxation generator represents a specially chosen RLC circuit with negative damping. The electrical relaxation oscillation observed by Nagumo [NAY62] in the electrical circuit with the tunnel diode had a similar mathematical description to the equation for the Van der Pol relaxation oscillator. FitzHugh [Fit69] modified Van der Pol and Nagumo equations in such a way that they qualitatively described the processes of generation and propagation of electrical pulses in nerve fiber. These equations, now known as FitzHugh-Nagumo, were further modified to simulate the processes in the heart muscle. The straight-line approximation of non-linear functions in this mathematical model introduced in [KK73] allows us to find analytically a number of important dependencies related to the generation and propagation of AP in heart muscle. Recently, Kogan et al. showed how to incorporate the APD restitution properties of heart muscle cells into this model [KKB91b], and proved that the result obtained with this model in spiral wave propagation qualitatively reflects the behavior of spiral wave in vitro experiment [PDS93]. The FH-N model can also be considered as an ionic simplified model, where the fast variable plays the role of generalized inward current and the slow variable plays the role of the generalized outward current which is controlled by the generalized gate variable.

# CHAPTER 3

# Investigation of the Existing Simplified Models

## 3.1 General Considerations

The well-known detailed ionic models of AP (old Noble [Nob62] and recent Luo-Rudy [LR91]) are too complicated for the computer simulation of excitation wave propagation along heart muscles. Therefore, a wide spectrum of simplified models was developed. To be useful for AP propagation study, these models have to correctly reproduce the global characteristics of AP ($\left(\frac{dE}{dt}\right)_{max}$ – the maximum speed of depolarization, $D$ – AP duration, $E_{max}$ – amplitude of AP) and the cell recovery processes (which are developed when the AP is returned to its rest value) inherent in the detailed model.

The simplification of the full mathematical model of AP generation is based on two assumptions:

**1.** The gate variables $m$ and $h$, which determine the conductivity of the membrane for the sodium current in the full model, are changing so rapidly that it is possible to assume that they reach their steady state values $m_\infty(E)$ and $h_\infty(E)$ instantaneously. For the Noble model, it was proved [KK73], using singular perturbation theory, that this assumption is correct. This assumption causes a decrease of the maximal rate of depolarization which can be easily compensated by decreasing the membrane capacity or by increasing the maximum value of the inward current. From here on, the total ionic current is divided into two components: inward current $I_{inw}$ which flows from outside to inside the cell, and outward current $I_{outw}$ which flows from inside to outside the cell.

**2.** The total outward current being a function of membrane potential $E$ and time $t$ can be represented as a product of two functions: a function of one variable $E$, representing the dependence of steady state generalized outward current on membrane potential $E$, and a function of two variables $E$ and $t$, representing the generalized gate variable for the generalized outward current:

$$I_{outw}(E,t) = Y^k(E,t)I_{outw}(E)$$

Here, $Y$ is the dimensionless generalized gate variable for outward current ($0 \leq Y \leq 1$), $k$ is a constant; usually k is chosen as greater than unity to minimize the effect of outward current on the depolarization processes. For example, in the Noble equations $k = 4$.

This assumption excludes the time independent components of outward current inherent in physiological models (see [Nob62] and [LR91]). These components are responsible for the first part of the repolarization phase of AP and, particularly, for the overshoot. Therefore, this assumption introduces additional errors in the reproduction of AP.

The generalized gate variable $Y(E,t)$ is obtained as a solution of the equation:

$$\tau_Y \frac{dY}{dt} = Y_\infty(E) - Y \tag{3.1}$$

The Noble equations show that only one gate variable $n$ does not reach its steady state value after the completion of the repolarization processes. The transient of that gate variable during diastole determines the APD restitution curve – a very important determinant of repeatable wave propagation. This transient can not be described properly by (3.1) with $\tau_Y = const.$ $\tau_Y$ must be a function of $E$ and $\frac{dY}{dt}$:

$$\tau_Y = \begin{cases} \tau_1 & \text{if } \frac{dY}{dt} > 0 \\ \tau_1 K_1 & \text{if } \frac{dY}{dt} < 0, Y > Y_{lim} \\ \tau_1 K_2 & \text{otherwise} \end{cases}$$

The value of $\tau_1$ determines the AP duration and, under normal conditions, is 100 times greater than the time constant of the fast variable $E$. The coefficient $K_2$ can be found directly from the given APD restitution curve (see [KKB91b, KKK96, KKK95a]), and $K_1$ and $Y_{lim}$ are established in the process of final adjustment of this restitution curve. The function $Y_\infty(E)$ has to be equal to zero when $E = E_{rest}$ and equal to 1 when $E = E_{max}$. Inside this $[E_{rest}, E_{max}]$ range of $E$ any rough stepwise or piecewise linear approximation can be used (see, for example, Fig. 3.1). The effect of $n$ on $\left(\frac{dE}{dt}\right)_{max}$ of the next AP is negligible.

Therefore, the general form of the simplified model based on the Noble formulation [Nob62] and the above mentioned assumptions is:

$$C\frac{dE}{dt} = -I_{inw}(E) - \left(\frac{Y}{Y_B}\right)^k I_{outw}(E) \tag{3.2}$$

$$\tau_Y(E)\frac{dY}{dt} = Y_\infty(E) - Y \tag{3.3}$$

with initial conditions: $E(0) = E_{rest}, Y(0) = 0$. Here $Y$ is a generalized gate variable. The introduction of the ratio $\left(\frac{Y}{Y_B}\right)^k$ instead of $Y^k$ following Karma [Kar93] permits the adjustment of parameters $Y_B$ and $k$ to control the action potential duration and the shape of the AP during the last part of repolarization phase.

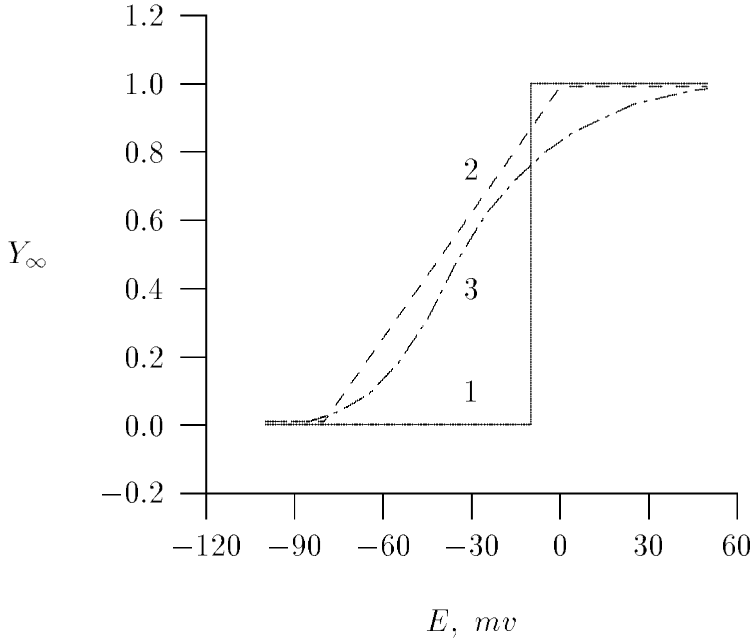


Figure 3.1: The $Y_\infty$ curves used in the Karma model (1), in the Van Capelle – Durrer model (2), and in the Noble model (3).

The behavior of the models described by the general equations (3.2) and (3.3) can be analyzed using $I_{inw}(E)$ and $I_{outw}(E)$ plots and some general properties of the AP. Indeed, the slope of AP in any given point of time is completely determined by the difference between $I_{inw}(E)$ and $\left(\frac{Y}{Y_B}\right)^k I_{outw}(E)$. During the depolarization phase, $\left(\frac{Y}{Y_B}\right)^k \approx 0$, and the outward current does not affect the depolarization processes. If $\left(\frac{Y}{Y_B}\right)^k$ continues to be zero after $I_{inw}(E) = 0$ or $I_{inw}(E) = \left(\frac{Y}{Y_B}\right)^k I_{outw}(E)$, we obtain a plateau without overshoot. To obtain fast repolarization, the following has to be true: $\left(\frac{Y}{Y_B}\right)^k I_{outw}(E) > I_{inw}(E)$.

Another form of the generalized second order simplified model can be obtained if $I_{outw}$ in (3.2) is represented as a sum of two components $I_{outw} = -I_{inw} + \Delta I_{outw}$

$$C\frac{dE}{dt} = -I_{inw}(E)[1 - \left(\frac{Y}{Y_B}\right)^k] - \left(\frac{Y}{Y_B}\right)^k \Delta I_{outw} \tag{3.4}$$

$$\tau_Y(E)\frac{dY}{dt} = Y_\infty(E) - Y \tag{3.5}$$

The current $\Delta I_{outw}$ can be synthesized (as a piecewise-linear function) to reproduce the desired shape of the repolarization phase of the AP. $I_{inw}$ can be obtained from experimental data.

Using these general considerations we analyze the most widely used simplified models.

## 3.2 FitzHugh – Nagumo Model

The FitzHugh-Nagumo model is the simplest of the existing simplified models. The equations which describe this model when reduced to dimensionless form [PCP81] are:

$$\begin{aligned}
\frac{\partial E}{\partial t} &= \Delta E + F(E) - I + I_{stim} \\
\frac{\partial I}{\partial t} &= \varepsilon(E)[f(E) - I]
\end{aligned} \tag{3.6}$$

where $E$ – fast variable (membrane potential displacement between the interior and exterior of the cell), $I$ – slow variable (generalized outward current), $\Delta = \partial^2/\partial x^2 + \partial^2/\partial y^2$ – two dimensional Laplacian operator, $F(E)$ – current-voltage characteristic of the fast inward current, $f(E)$ – current-voltage characteristic of the slow outward current, $\varepsilon(E)$ – small parameter (inversely proportional to the time constant of the slow outward current). The piecewise-linear approximation of the functions $F(E)$ , $f(E)$ , and $\varepsilon(E) = 1/\tau_Y(E)$ is shown on Fig. 3.2.

To solve equations (3.6), it is necessary to choose the appropriate initial and boundary conditions.

Let us reduce equations (3.6) to the general form given by (3.2) and (3.3).

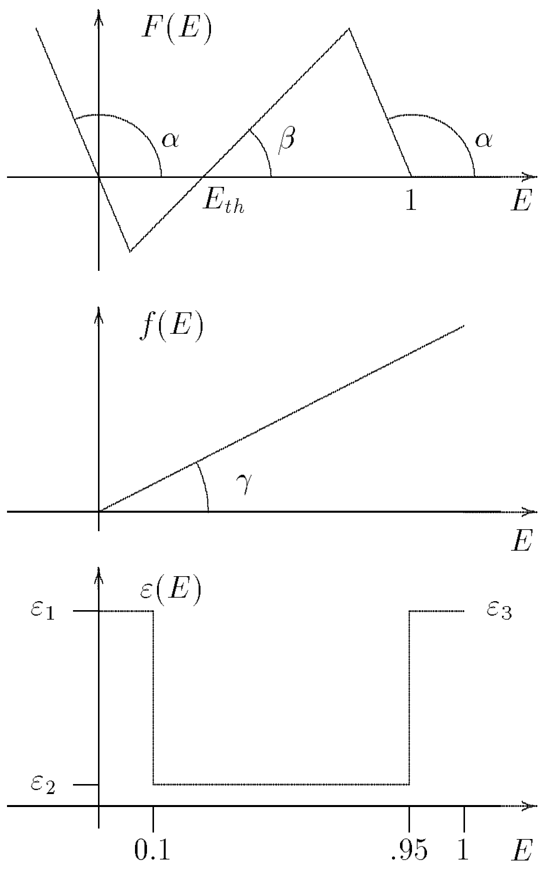


Figure 3.2: The piece-wise linear approximation of functions $F(E)$, $f(E)$, and $\varepsilon(E)$. $\tan\alpha = G_r$; $\tan\beta = G_f$; $\tan\gamma = G_s$; $E_{th}$ – the threshold potential.

After introducing the substitutions $I = Yf_1(E)$ and $f(E) = Y_\infty(E)f_1(E)$ in (3.6) we obtain

$$\begin{aligned} \frac{\partial E}{\partial t} &= \Delta E + F(E) - Yf_1(E) + I_{stim} \\ \frac{\partial Y}{\partial t} &= \varepsilon(E)[Y_\infty(E) - Y] \end{aligned} \tag{3.7}$$

Here $Y_\infty(E)$ is a step function of $E$; $F(E)$ and $Yf_1(E)$ can be considered as the generalized inward and outward currents. In Fig. 3.3, these currents are shown as functions of $E$. The graph shows that after the end of the depolarization phase, the action potential will have an abnormally prolonged phase of plateau

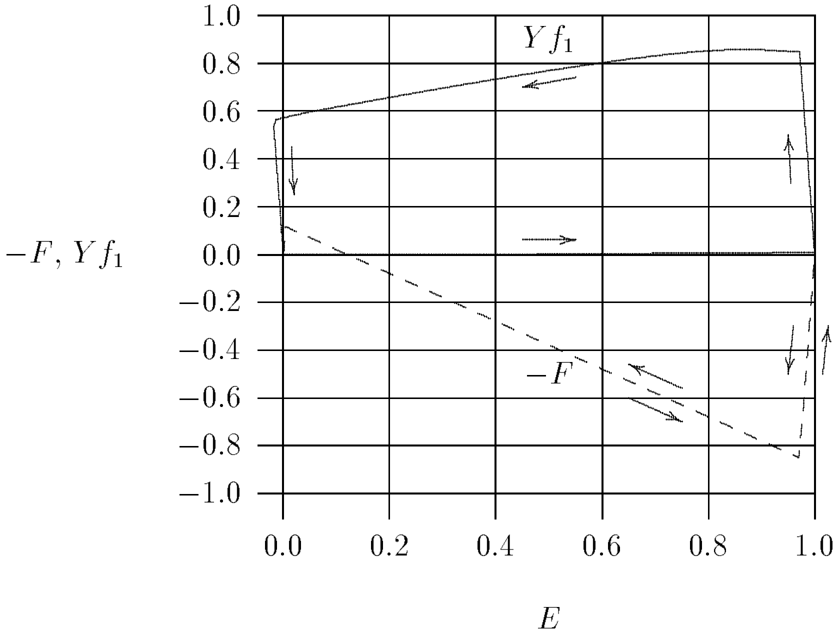


Figure 3.3: Functions $-F(E)$ and $Yf_1(E)$ for the FH-N model. The arrows pointing from left to right designate the changes of the inward ($-F(E)$) and outward ($Yf_1(E)$) currents in the depolarization phase of AP, and arrows pointing in the opposite direction show the changes of the same currents in the repolarization phase.

and a short fast repolarization phase.

The widely used set of parameters for this model (see [PCP81, PP81, NW87, EPS89, PEP84, Win87, Win89]), hereafter referred to as the standard set, is: $G_s = 1$, $G_f = 1$, $G_r = 30$, $E_{th} = 0.16$,

$$\varepsilon(E) = \begin{cases} \varepsilon_1 = 0.5 & \text{if } 0.00 < E < 0.01 \\ \varepsilon_2 = 0.01 & \text{if } 0.01 \le E \le 0.95 \\ \varepsilon_3 = 0.5 & \text{if } E > 0.95 \end{cases} \tag{3.8}$$

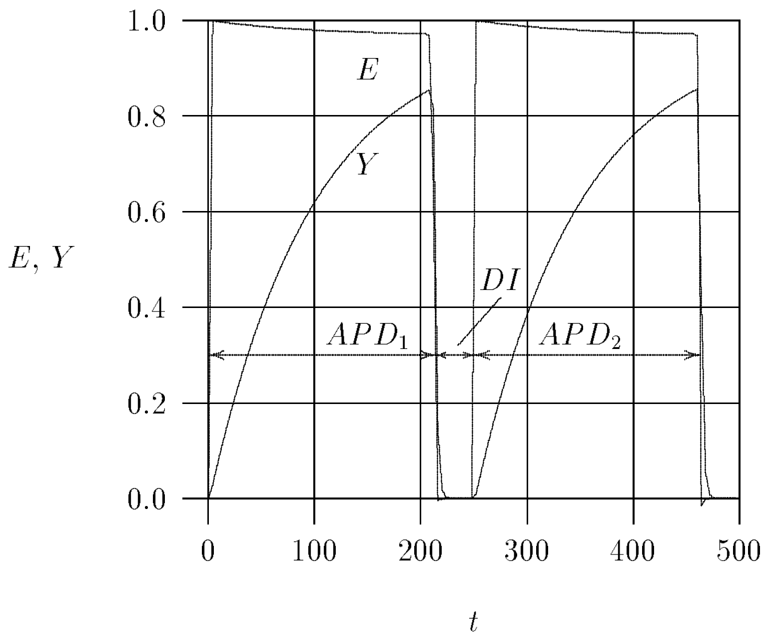


Figure 3.4: The $E(t)$, and $Y(t)$ for the short diastolic interval. $DI/APD_1 = 0.234$; $APD_2/APD_1 = 1$ (in the model presented in [PCP81]).

The relationships between the action potential duration, refractory period (R), and the model parameters $G_s$ , $G_f$, and $\varepsilon$ are presented in [PCP81] for the model without diffusion (point model). These dependencies qualitatively reflect the essential properties of heart muscle cells, but do not correctly express the restitution properties and the shape of the AP.

The transients of $E$ and $Y$ in a cardiac cycle with a small $DI$ are shown in Fig. 3.4 for the standard parameters of the FH-N simplified model. Note that the slow variable $Y$ reaches zero almost immediately after the AP returns to the resting potential. Thus, a stimulus applied after a short $DI$ produces a subsequent AP of approximately the same duration as the previous one, because the gate variable $Y$ when $\frac{dY}{dt} < 0$ almost instantaneously decreases (see Fig. 3.4). The original APD restitution curve in the FH-N model is very steep (see Fig. 3.5 curve

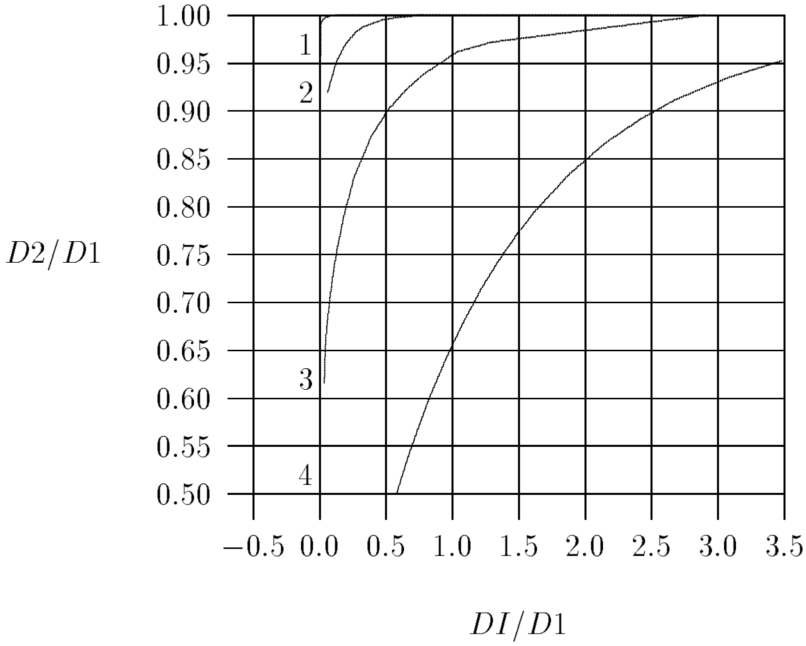


Figure 3.5: The restitution curves in normalized form obtained for the original FitzHugh – Nagumo model (1), for the Van Capelle – Durrer model (2), for the Luo-Rudy model (3), and for the Karma model (4).

1) and differs much from the experimental curve (Fig. 3.5 curve 3). Therefore, a method was developed to modify the function $\varepsilon(E)$ so as to fit the experimental APD restitution curve.

Expression (3.8) can now be written as (see [KKB91b] for details)

$$\varepsilon(E) = \begin{cases} \varepsilon_1 & \text{if } E < 0.01 \text{ and } \frac{dY}{dt} > 0 \\ \\ \varepsilon_2 & \text{if } E \geq 0.01 \text{ and } \frac{dY}{dt} > 0 \\ \\ \varepsilon_3 & \text{if } Y > Y_{min} \text{ and } \frac{dY}{dt} \leq 0 \\ \\ \varepsilon_4 = k\varepsilon_2 & \text{otherwise} \end{cases} \tag{3.9}$$

## 3.3 Van Capelle – Durrer Model

The Van Capelle and Durrer model [VD80] can be derived from general equations (3.4) – (3.5) as follows: we rename $I_{inw}$ as $-f$ and $\Delta I_{outw}$ as $i_1$, and then replace in equation (3.4), the term $1-\left(\frac{Y}{Y_B}\right)^k$ with $(1-Y)$, $\left(\frac{Y}{Y_B}\right)^k$ with 1, and set $\tau_Y(E) = T = const$ in equation (3.5). As a result we get:

$$\begin{aligned} C\frac{dE}{dt} &= (1-Y)f(E) - i_1(E) \\ T\frac{dY}{dt} &= Y_\infty(E) - Y \end{aligned}$$

The functions $(1-Y)f(E)$ and $i_1(E)$ are represented in Fig. 3.6 in the form proposed by VC-D [VD80]. The figure clearly shows that the maximal rate of $\frac{dE}{dt}$ in the depolarization phase can be determined by:

$$\begin{aligned} \left(\frac{dE}{dt}\right)_{max} &= \frac{(1-Y)f(E_a) - i_1(E_a)}{C} \qquad or \\ \left(\frac{dE}{dt}\right)_{max} &= \frac{f(E_a)}{C} - \frac{Yf(E_a) + i_1(E_a)}{C} \end{aligned} \tag{3.10}$$

$E_a$ is the value of membrane potential at which $\frac{dE}{dt}$ reaches its maximum value. The first term on the right side of the equation (3.10) represents the ideal value

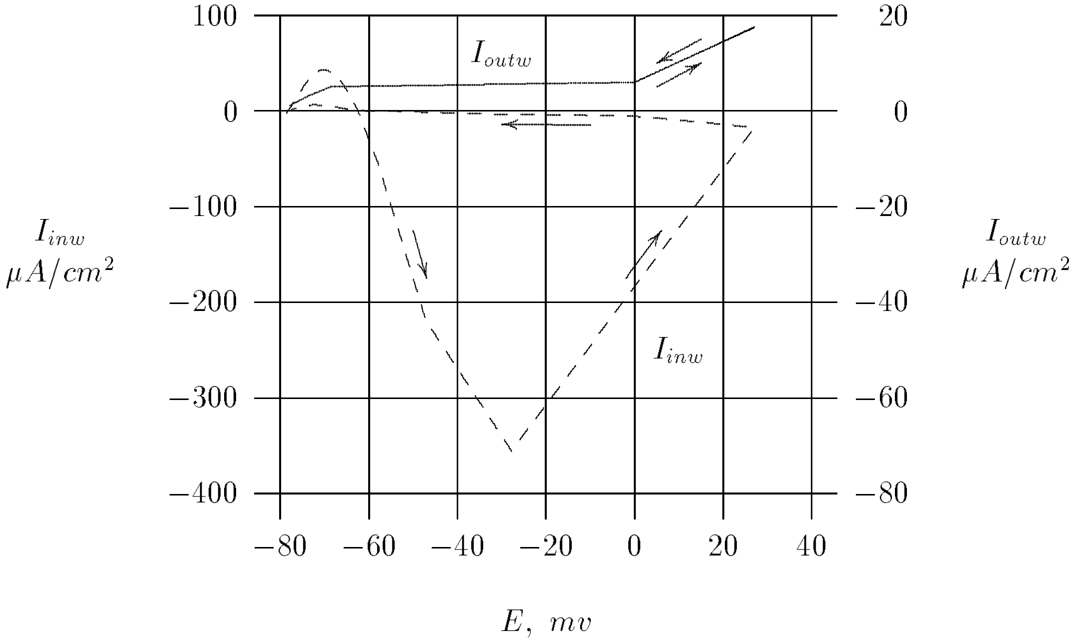


Figure 3.6: $I_{inw} = (1 - Y)f(E)$ and $I_{outw} = i_1(E)$ currents for the VC-D model. The arrows pointing from left to right designate the changes of the inward and outward currents in the depolarization phase of AP, and arrows pointing in the opposite direction show the changes of the same currents in the repolarization phase.

of $\left(\frac{dE}{dt}\right)_{max}$, and the second term is the error introduced by the VC-D model. The error grows with the increasing values of $Y$ and $i_1(E_a)$. This occurs in the case of repetitive stimulation (increase of $Y$) and when a decrease of APD is achieved by an increase of $i_1$.

The replacement of $\tau_Y(E)$ with $T = const$ leads to the error in the reproduction of the APD restitution properties (see Fig. 3.5 curve 2). This error and the error in $\left(\frac{dE}{dt}\right)_{max}$, inherent in the VC-D model, affect the velocity of wave propagation and, therefore, restrict the domain of the applicability of this model.

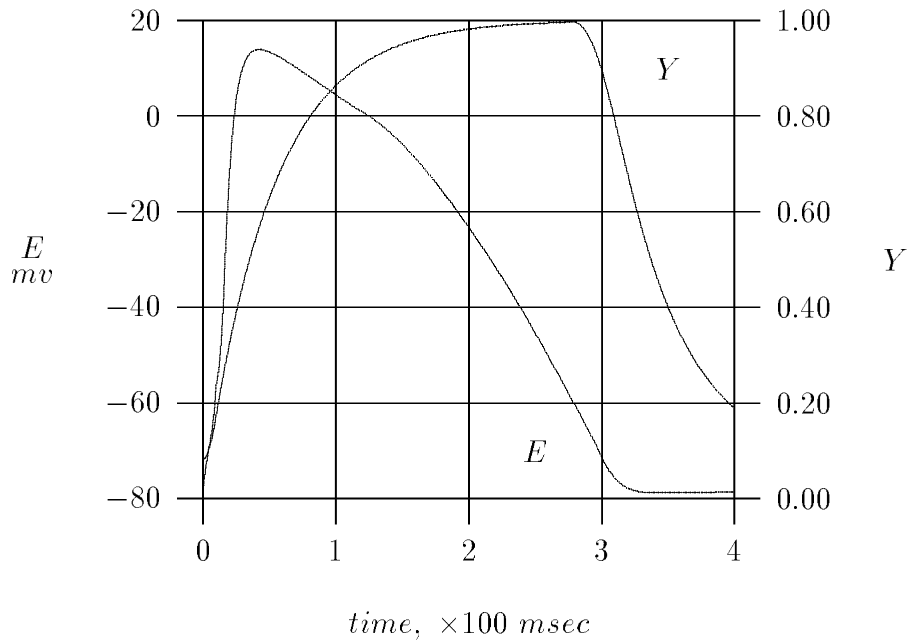


Figure 3.7: The AP and gate variable $Y$ as functions of time in the VC-D model.

The transient of the AP and gate variable $Y$ for the VC-D model are shown in Fig. 3.7.

## 3.4 Karma Model

This model [Kar93] is a simplification of the Noble model [Nob62]. It has three essential properties of the Noble model that are missing in the original FitzHugh-Nagumo model:

1. Insensitivity of $\left(\frac{dE}{dt}\right)_{max}$ to changes of the slow gate variable $n$ in the case of repeatable excitation,

2. The fast repolarization period is much longer than the fast depolarization period,

3. There is an alternation in APD in case of repeatable excitation.

The two-variable model equations in the dimensionless form proposed by Karma [Kar93] are:

$$\begin{aligned}
\varepsilon \frac{\partial E}{\partial t} &= \varepsilon^2 \nabla^2 E - E + [A - \left(\frac{n}{n_B}\right)^M] \\
&\qquad \times [1 - tanh(E-3)] \frac{E^2}{2} \\
\frac{\partial n}{\partial t} &= \Theta(E-1) - n, \qquad (3.11)
\end{aligned}$$

where $\Theta(x)$ is the standard Heaviside step-function; $\varepsilon$, a small parameter characterizing the abruptness of excitation; $A$, a constant; $\nabla^2$, Laplacian of appropriate dimension; $n$, slow gate variable equivalent to $Y$ in (3.2).

Typical values of the parameters are $A = 1.5415, M = 30, n_B = 0.507, \varepsilon = 0.009$.

Let us reduce the equations (3.11) to the generalized form. For this purpose, consider the isolated cell $\nabla^2 E = 0$. After defining $f(E) = [1 - tanh(E-3)]\frac{E^2}{2}$ and $n_\infty(E) = \Theta(E-1)$, and substituting $\bar{t} = t/\varepsilon$; $T = 1/\varepsilon$ into (3.11) we finally get:

$$\begin{aligned}
\frac{dE}{d\bar{t}} &= [Af(E) - E] - \left(\frac{n}{n_B}\right)^M f(E) \\
T\frac{dn}{d\bar{t}} &= n_\infty(E) - n \qquad (3.12)
\end{aligned}$$

In these equations $Af(E) - E$ corresponds to the inward current and the product $\left(\frac{n}{n_B}\right)^M f(E)$ corresponds to the outward current. So,

$$\begin{aligned}
\frac{dE}{d\bar{t}} &= I_{inw}(E) - I_{outw}(E,t) \\
T\frac{dn}{d\bar{t}} &= n_\infty(E) - n \qquad (3.13)
\end{aligned}$$

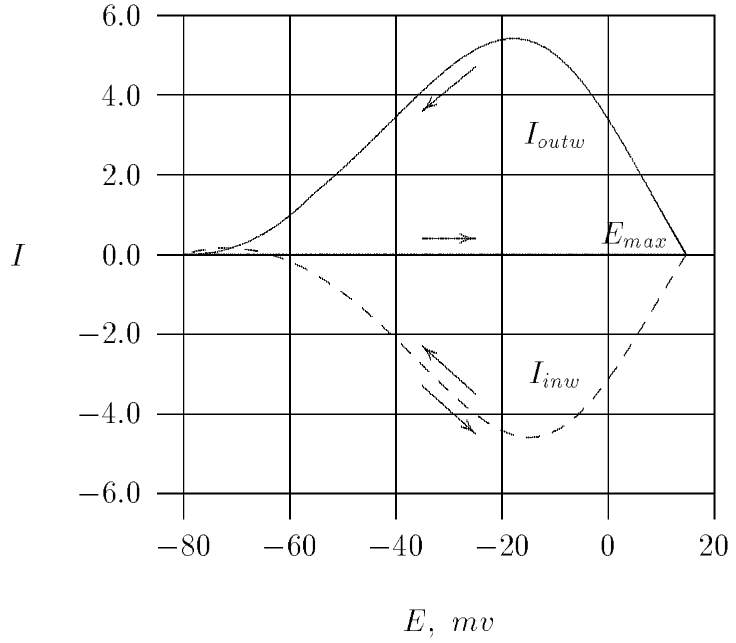


Figure 3.8: $I_{inw} = -(Af(E) - E)$ and $I_{outw} = \left(\frac{n}{n_B}\right)^M f(E)$ currents for the Karma model. The arrows pointing from left to right designate the changes of the inward and outward currents in the depolarization phase of AP, and arrows pointing in the opposite direction show the changes of the same currents in the repolarization phase.

In Fig. 3.8, $I_{inw}(E) = -(Af(E) - E)$ and $I_{outw}(E,t) = \left(\frac{n}{n_B}\right)^M f(E)$ are shown in the course of AP generation (Fig. 3.9). During the depolarization phase, $I_{inw}$ traces the bottom curve in the direction of arrows from left to right. At the same time, $I_{outw} = 0$ due to $\left(\frac{n}{n_B}\right)^M \ll 1$ (the arrows along $x$ axis). Therefore, in the case of repeatable excitation with small but finite diastolic intervals, the outward current does not affect the depolarization processes and especially $\left(\frac{dE}{dt}\right)_{max}$. A growth of $[Af(E)]_{max}$ will cause a rise of $\left(\frac{dE}{dt}\right)_{max}$. After $I_{inw}$ becomes equal to 0, and $E$ reaches $E_{max}$, the repolarization phase begins. Due to the small excess of outward current, the membrane potential begins to decrease at a slow rate,

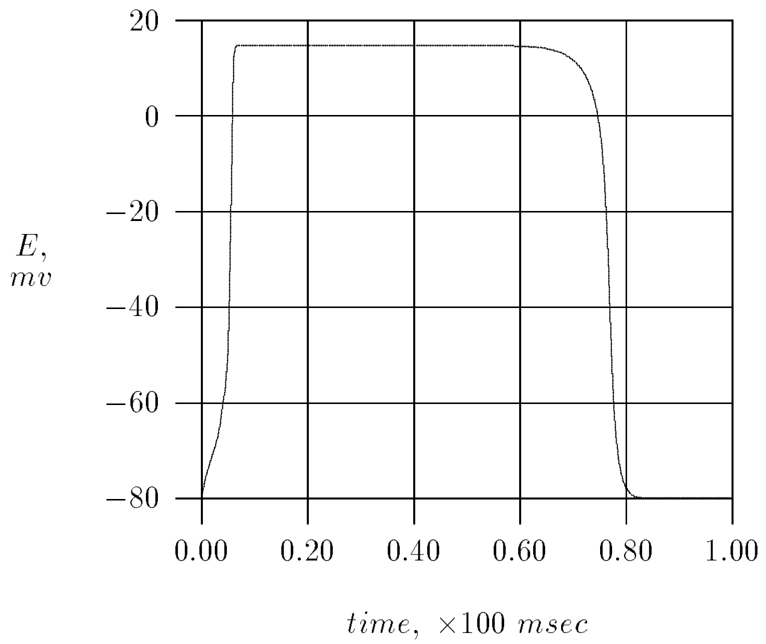


Figure 3.9: AP generated by the Karma model.

producing in the time domain something resembling a plateau. The duration of this phase depends on the value of the time constant T in (3.13) (which determines the change of the variable $n$ with respect to time), as well as on parameters $A$, $n_B$ and $M$. In Fig. 3.8, this region is located in the vicinity of the point $E_{max}$. The development of the repolarization process is shown by arrows on the $I_{inw}$ and $I_{outw}$ curves. Fig. 3.8 and equation (3.12) lead to the conclusion that the greater is $T$ or $A$, the longer is the period of slow repolarization. With the decrease of the parameter $n_B$, the period of slow repolarization as well as the APD shorten. When $n \geq n_B$, the excess of the outward current over the inward current increases in time, resulting in a smooth increase of the repolarization rate, until its maximum value is reached. When the AP is close to $E_{rest}$, this excess decreases together with $f(E)$, and AP slowly approaches $E_{rest}$. Parameter $n_B$ also affects the APD restitution curve. The APD restitution curve (4) on Fig. 3.5

corresponds to $n_B = 0.507$.

## 3.5 Conclusion

The existing simplified models exhibit the following properties:

1. All of them are based on the same assumptions and differ in the analytical approximations of the experimental dependencies of $I_{inw}(E)$ and $I_{outw}(E)$, and in the way the slow variable affects the outward current.

2. In comparison with the electrophysiological models, they all produce decreased $\left(\frac{dE}{dt}\right)_{max}$ (due to the substitution $h = h_\infty$, $m = m_\infty$) and introduce time constants of slow variable, $T$, that do not depend on $E$. This independence leads to substantial errors in reproducing the APD restitution.

3. In all simplified models considered here, the time independent component of the outward current is neglected. That excludes the overshoot in generated AP. The VC-D model is an exception, where overshoot can be obtained by changing the slope of the last segment of piece-wise linear approximation of current $i_1$.

4. Analysis of the Beeler-Reuter [BR77] and Luo and Rudy physiological models shows that the gate variable $j$ in the case of a short diastolic interval does not return to its steady state value $j = 1$. That decreases the $\left(\frac{dE}{dt}\right)_{max}$ of the depolarization phase of the next AP and correspondingly decreases the velocity of the repeatable wave propagation. This phenomenon is not reproduced by the second-order simplified models.

# CHAPTER 4

# The Third-Order Simplified Model

The analysis of the simplified models presented in the previous chapter shows that all of them are based on the same assumptions and old physiological data used in the Noble model. They produce a decreased maximal rate of depolarization and do not reproduce properly the cell recovery processes and the shape of AP. Some attempts were made to install the experimental APD restitution data onto the FH-N model [KKB91b] and to artificially adjust the steepness of the APD restitution and dispersion curves in the Karma model [Kar94]. Both improvements do not solve the global problem of creating the simplified model based on modern physiological data, nor are they capable of correctly reproducing the recovery processes.

This chapter is focused on the synthesis of a simplified model which would correctly reproduce the global characteristics of AP and the cell recovery processes important for computer simulation of AP propagation in heart muscle tissue. The first version of this model is based on the modern data used in the sophisticated physiological model proposed by Luo and Rudy [LR91].

## 4.1 The Analysis of the Luo and Rudy Model

**General considerations** For any cell membrane we have:

$$-C\frac{dE}{dt} = I_{total} \tag{4.1}$$

where $C$ – membrane capacitance, $E$ – transmembrane potential, $I_{total}$ – total current through the membrane.

The total current can be divided into three components: general inward ionic current $I_{inw}(E,t)$, general outward ionic current $I_{outw}(E,t)$, and external current produced by a stimulus and neighboring cells $I_{ext} = I_{stim} + I_n$. The current from the neighboring cells, when heart muscle tissue is considered as a syncytium, is determined by the Laplacian of the appropriate dimension. Thus, the equation for AP generation and propagation takes the general form

$$-C\frac{\partial E}{\partial t} = I_{inw} + I_{outw} + I_{stim} + \alpha_x\left(\frac{\partial^2 E}{\partial x^2} + A_1\frac{\partial^2 E}{\partial y^2} + A_2\frac{\partial^2 E}{\partial z^2}\right) \tag{4.2}$$

Here $\alpha_x$ represents intracellular conductivity in the fiber longitudinal direction, $A_1, A_2$ determine anisotropy ratios of the tissue.

Following the Hodgkin - Huxley formalism, different and increasingly complicated analytical expressions for inward and outward currents of heart cells were proposed. For example, the LR model of ventricular cardiac action potential, introduced in 1991 [LR91], gives a more detailed description of the inward and outward currents, including the effects of $[Ca]_i$ and $[K]_o$ changes:

$$I_{inw}(t,E) = I_{Na} + I_{si} \tag{4.3}$$

$$I_{Na}(t,E) = 23m^3hj(E - E_{Na}) \tag{4.4}$$

$$I_{si}(t,E) = 0.09df(E - E_{si}) \tag{4.5}$$

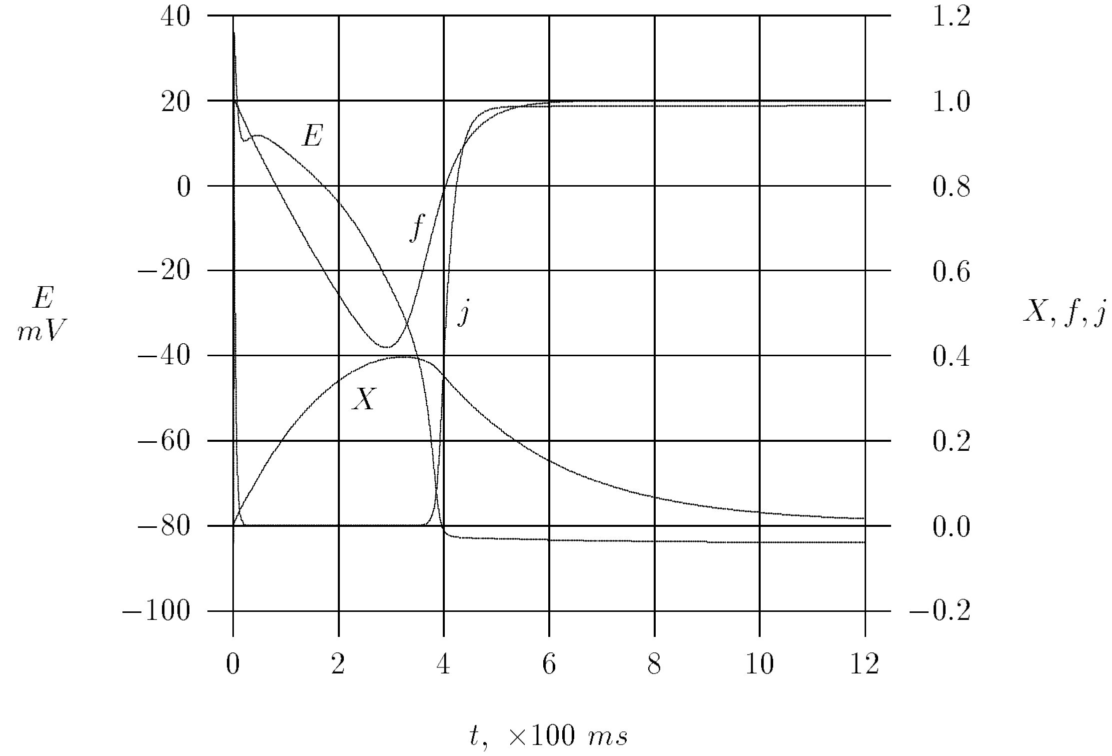


Figure 4.1: The AP and gate variables $X$, $f$, and $j$ as functions of time.

$$E_{si} = 7.7 - 13.0287 ln([Ca]_i) \quad (4.6)$$

$$\frac{d[Ca]_i}{dt} = -10^{-4} I_{si} + 0.07(10^{-4} - [Ca]_i) \quad (4.7)$$

$$I_{outw}(t, E) = I_K + I_{K_{1_{(T)}}} = \bar{g}_K X(E,t) X_i(E)(E - E_K) + I_{K_{1_{(T)}}}(E) \quad (4.8)$$

Here $m, h, j, d, f, X$ are the gate variables determined by

$$\tau_y(E)\frac{dy}{dt} = y_\infty(E) - y; \quad y = m, h, j, d, f, X \quad (4.9)$$

Details of the LR model can be found in their original publication [LR91].

**Computer simulation** of the LR model shows that under normal conditions the global characteristics of the generated AP are: APD at the level of 90% $E_{max}$ is 384 $ms$, $(dE/dt)_{max} = 344\ V/s$, $E_{max} = 110\ mV$, $E_{rest} = -84.2\ mV$. The recovery processes are characterized by the time behavior of the gate variables $j$, $f$, and $X$ after the completion of the AP repolarization phase (see Fig. 4.1). The residual part of gate variable $j$ is responsible for $(dE/dt)_{max}$ restitution, while gate variables $X$ and $f$ are responsible for APD restitution. The residual $j$ and $f$ variables are pronounced during the first $75 - 100\ ms$, the residual gate variable $X$ is present during most of the diastolic interval.

The AP depolarization phase is fully determined by the variation of sodium current (4.4), while the repolarization phase is determined by the summary effect of all other currents (4.5-4.8).

## 4.2 Synthesis of the Cardiac Cell Simplified Mathematical Model

The following considerations were used when developing the simplified cardiac cell model:

1. The detailed description of all ionic current components and corresponding membrane gate variables is not necessary for the adequate simulation of AP propagation. It is necessary to exactly reproduce only the AP characteristics which affect the speed of propagation ($(dE/dt)_{max}$, $E_{max}$, $D$) and the variables which characterize the cell recovery processes (APD restitution and $(dE/dt)_{max}$ restitution). The latter plays an important role when the cell is excited repeatedly.

2. The model must be based on the up-to-date physiological experimental data. This model is based on the data used in the sophisticated LR cardiac cell model and, therefore, can be considered as a LR model simplified for the

computer simulation of AP propagation.

3. In this model all ionic currents are combined into two groups: the currents participating in membrane depolarization and the currents involved in membrane repolarization.

4. In this model only the gate variables $j$ and $X$ are expressed explicitly as a solution of the corresponding ordinary differential equations.

With these considerations and for $\alpha_x = 0$ we obtain:

$$\begin{aligned}
-C\frac{dE}{dt} &= I_{dep}(E,t) + I_{rep}(E,t) + I_{stim} && (4.10)\\
I_{dep}(E,t) &= j(E,t)f_1(E) && (4.11)\\
I_{rep}(E,t) &= f_2(E) + X(E,t)f_3(E) && (4.12)\\
\tau_j(E)\frac{dj}{dt} &= j_\infty(E) - j && (4.13)\\
\tau_X(E)\frac{dX}{dt} &= X_\infty(E) - X && (4.14)
\end{aligned}$$

Here the time independent $f_1$, $f_2$ and $f_3$ correspond to the following currents in the LR model during the AP obtained for the normal conditions:

$$\begin{aligned}
f_1(E) &\longrightarrow I_{Na}(t,E) && (4.15)\\
f_2(E) &\longrightarrow I_{si}(t,E) + I_{K1}(E) && (4.16)\\
f_3(E) &\longrightarrow \bar{g}_K X_i(E)(E - E_K) && (4.17)
\end{aligned}$$

Functions $\tau_j(E)$, $j_\infty(E)$ and $X_\infty(E)$ are the same as in the LR model.

Thus, we reduce the original eighth-order LR model, with fifteen nonlinear functions, to a third-order model, with seven nonlinear functions. The functions $f_1$ and $f_2$ in our model are piece-wise approximated in six intervals by the second-order polynomials with the maximal relative error not exceeding 3.2 %. The

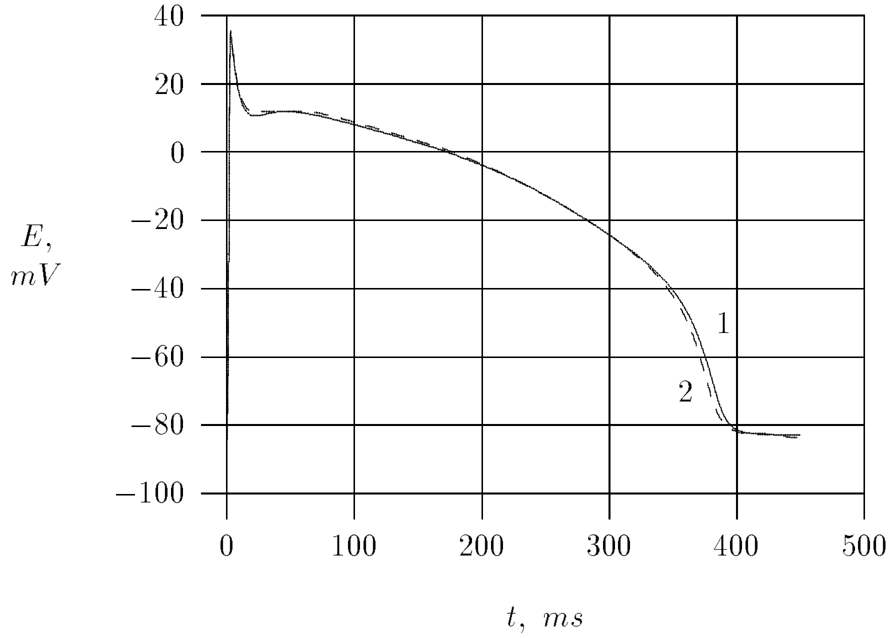


Figure 4.2: The shape of AP for the LR model (1) and for the third-order simplified model (2).

remaining five functions are calculated using analytical expressions provided by Luo and Rudy. The shape of the AP reproduced by the third-order simplified model and the LR model is shown in Fig. 4.2. The shapes of $I_{dep}$ and $I_{rep}$ for both models are presented in Fig. 4.3, 4.4. The relative errors in reproducing the global characteristics of AP by our model with respect to the LR model are: error in APD is 0.3 %, error in $(dE/dt)_{max}$ is 2.2 %, error in $E_{max}$ is negligible. To reduce the computation time we tabulated all seven functions with the uniform steps of $E$ equal to 1 $mV$ by simulating one AP using LR model and recording function values. In this case the errors were: 1.1 % for APD, 0.6 % for $(dE/dt)_{max}$ and 0.7 % for $E_{max}$. The time required for simulation of one AP in comparison with the original LR model was: 4.5 times less for the case of $f_1$ and $f_2$ piece-wise quadratic approximations, 19 times less for the case of tabulated functions. The

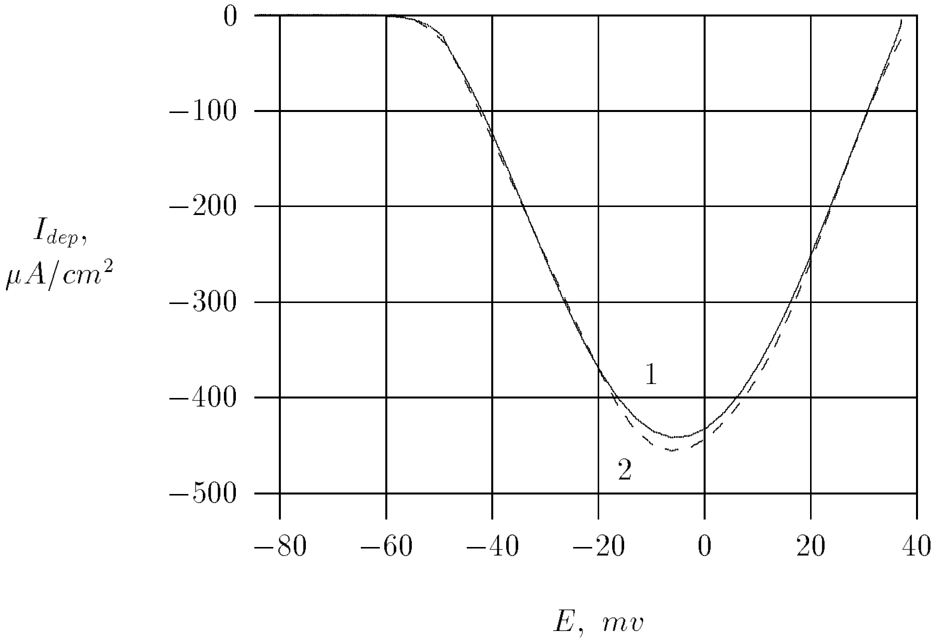


Figure 4.3: $I_{dep}$ current for the LR (1) and the third-order simplified (2) models.

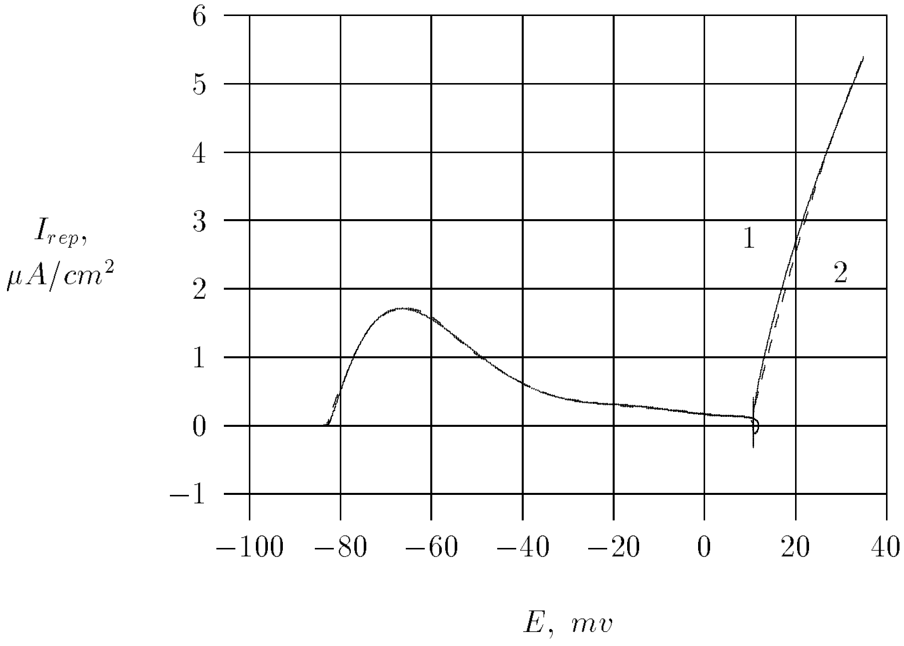


Figure 4.4: $I_{rep}$ current for the LR (1) and the third-order simplified (2) models.

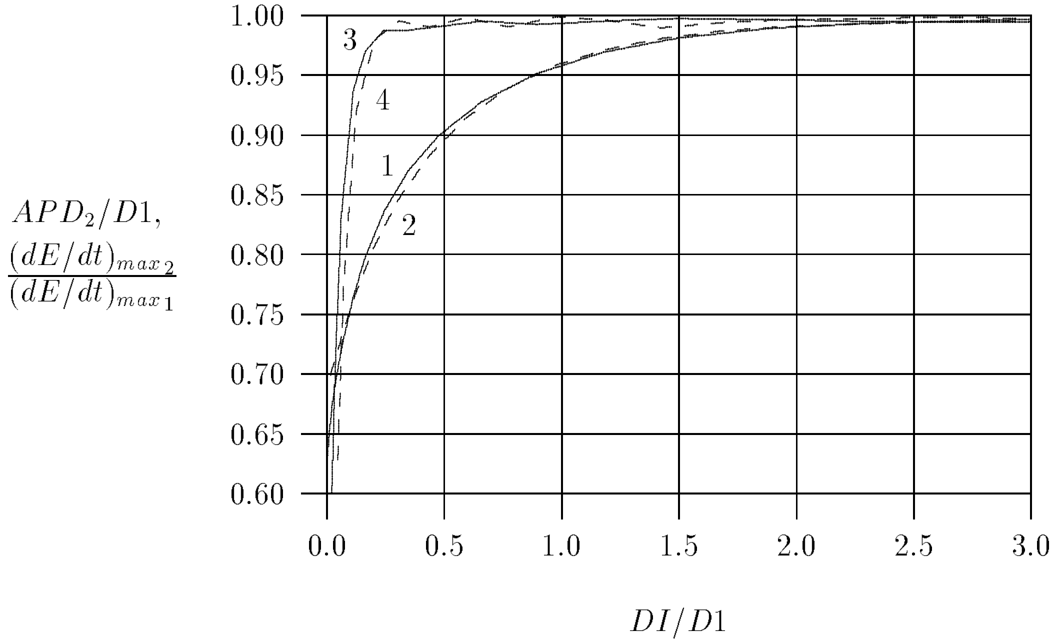


Figure 4.5: The restitution curves in normalized form obtained for the LR model (1,3) and for the third-order simplified model (2,4). 1,2 – APD restitution curves; 3,4 – $(dE/dt)_{max}$ restitution curves.

simulation was done on a Sun computer using the *gcc* compiler.

In order to take into consideration the effect of gate variable $f$ on APD restitution, the function $\tau_X$ is modified as follows:

$$\tau_X^*(E) = \begin{cases} 1.0\tau_X(E) & \text{if } dX/dt \geq 0 \\ 0.002\tau_X(E) & \text{if } dX/dt < 0, X \geq 0.23 \\ 0.85\tau_X(E) & \text{otherwise} \end{cases} \tag{4.18}$$

The APD restitution and $(dE/dt)_{max}$ restitution curves are shown in Fig. 4.5 together with those of the LR model. The APD restitution curves are in good

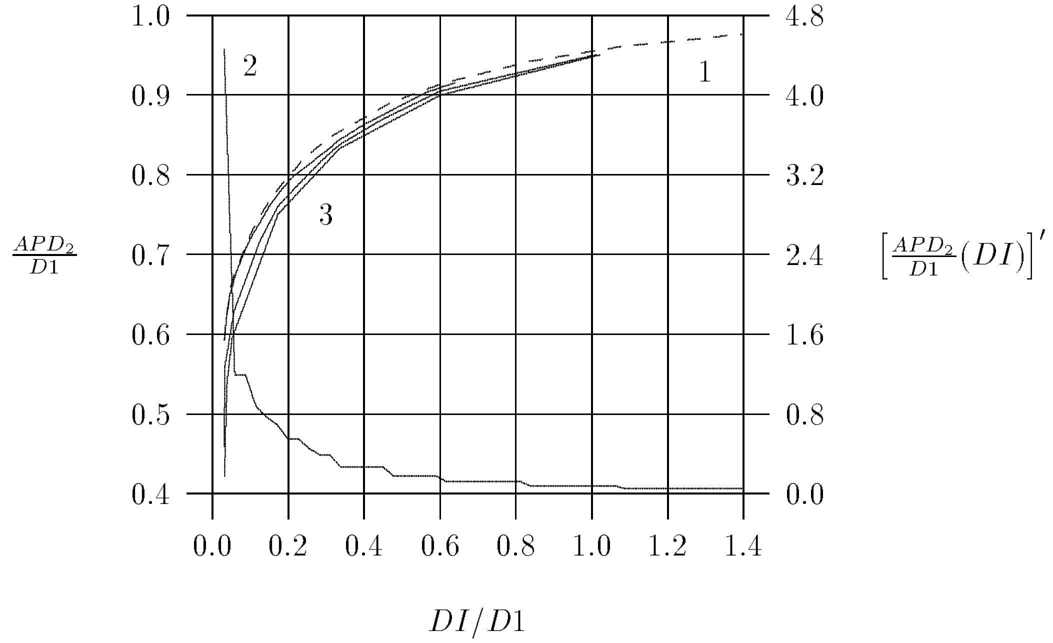


Figure 4.6: The APD restitution curve of the LR model obtained using S1,S2 protocol (1) and its derivative (2). A group of APD restitution curves of the LR model obtained using S1,S2,S3 protocol (3) with the $DI_1 = 20$ (lowest curve), 40 and 60 (highest curve) $ms$.

agreement and both have the slope not exceeding 1 for all realistic diastolic intervals.

The APD restitution curves obtained using S1, S2, S3 protocol are presented in Fig. 4.6, 4.7.

The shapes of AP during repeatable excitation are presented in Fig. 4.8 – 4.11 for periods of stimulation from $450ms$ to $600ms$. They show very little difference compared to the LR model.

Latest physiological studies [LR94] show that more realistic APD is $200ms$ as opposed to $400ms$ in the first version of LR model. Unfortunately, the published

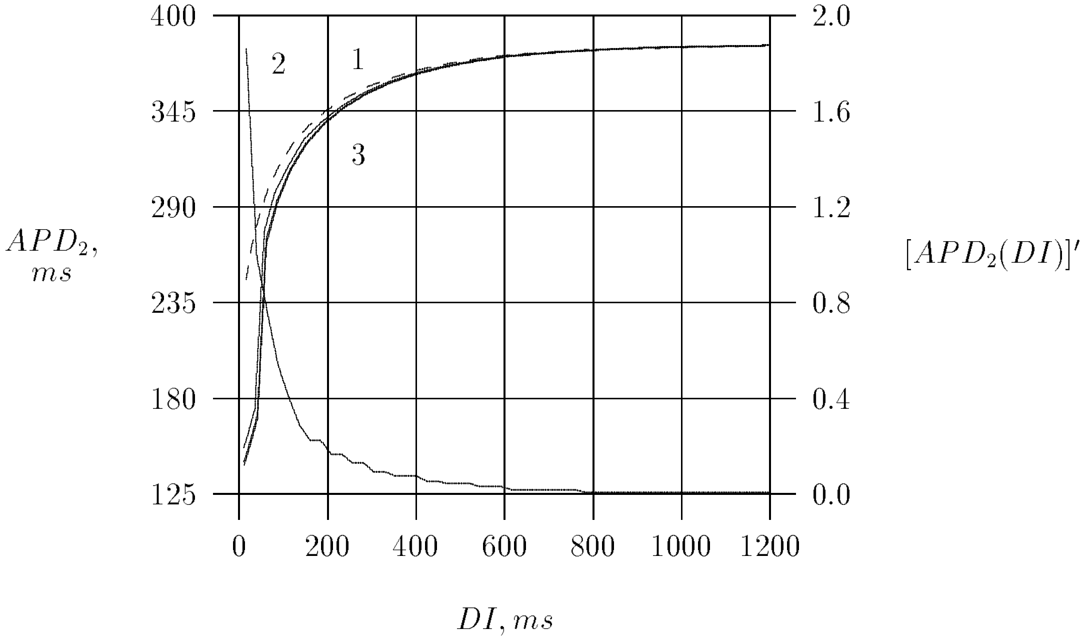


Figure 4.7: The APD restitution curve of the third-order model obtained using S1,S2 protocol (1) and its derivative (2). A group of APD restitution curves of the third-order model obtained using S1,S2,S3 protocol (3) with the $DI_1 = 20$ (lowest curve), 40 and 60 (highest curve) $ms$.

version of the LR II model [LR94] doesn't contain enough data for computer implementation. Therefore, the LR I model was modified to generate $200ms$ AP. It is possible to change the APD in the LR model by introducing two coefficients: $f_{I_K}$ for time-dependent repolarization current $I_K$, and $f_{I_{K1}}$ for sum of time-independent repolarization currents. The following values of these coefficients produced APD = $196ms$: $f_{I_K} = 6.0$, $f_{I_{K1}} = 1.7$.

After the adjustment, the tables of functions were rebuilt to transfer the changes into the simplified model. The drawback of this approach is that it changes the balance of currents in the model which distorts the restitution prop-

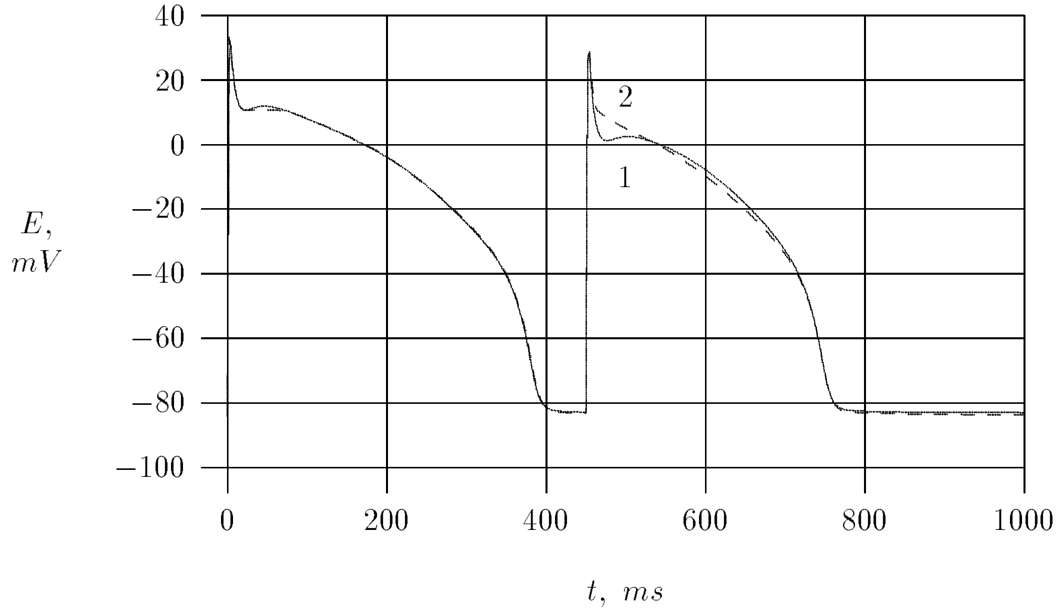


Figure 4.8: The shape of AP in case of repeatable excitation for the LR model (1) and for the third-order simplified model (2). $T_{stim} = 450ms$.

erties of the model. The method of restitution correction described above was not powerful enough to compensate for this distortion, so a new more efficient approach was proposed. This approach is based on the introduction of the coefficient $k_X$ for the $I_K$ as a function of the initial value of $X$ at the time of cell excitation. This dependence is tabulated to provide the required APD restitution curve for the model. This approach has the following advantages:

- any shape of the APD restitution curve can be obtained
- the $k_X(X_{init})$ table can be created automatically from the given APD restitution data using special program
- the APD restitution properties of the model can be easily changed by replacing the $k_X(X_{init})$ table

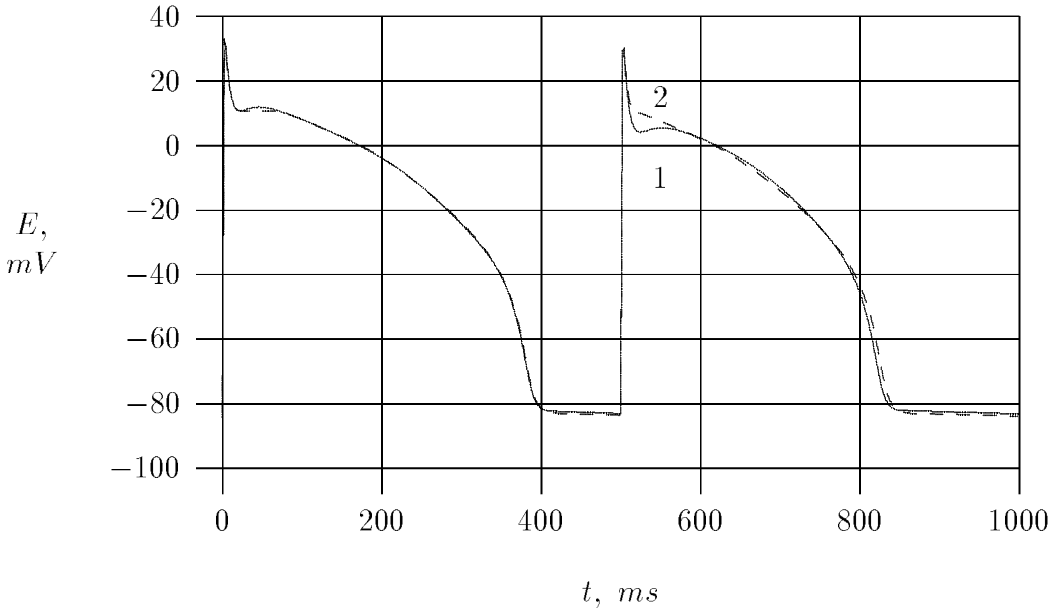


Figure 4.9: The shape of AP in case of repeatable excitation for the LR model (1) and for the third-order simplified model (2). $T_{stim} = 500ms$.

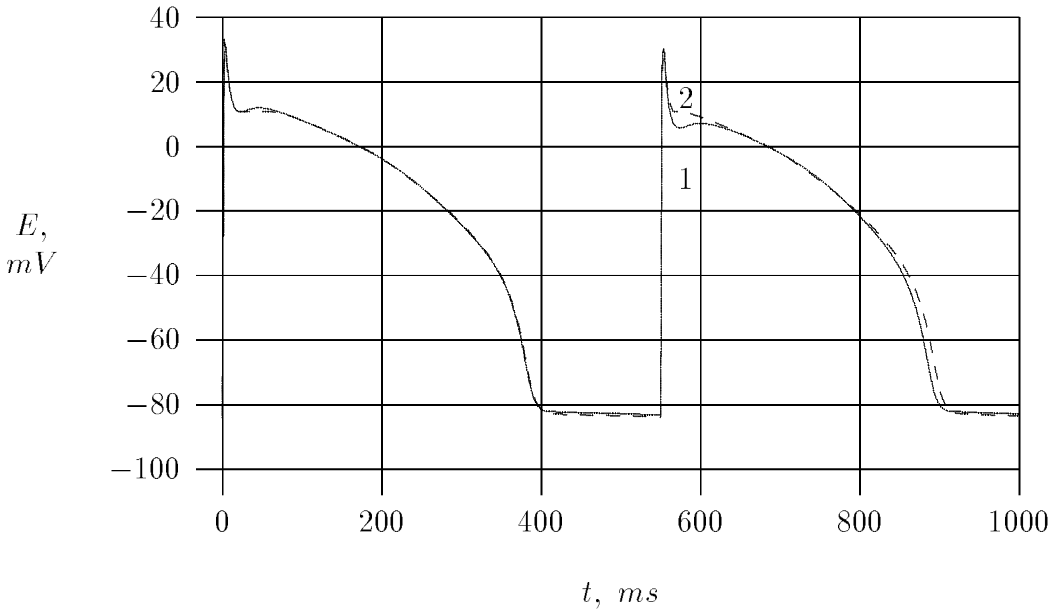


Figure 4.10: The shape of AP in case of repeatable excitation for the LR model (1) and for the third-order simplified model (2). $T_{stim} = 550ms$.

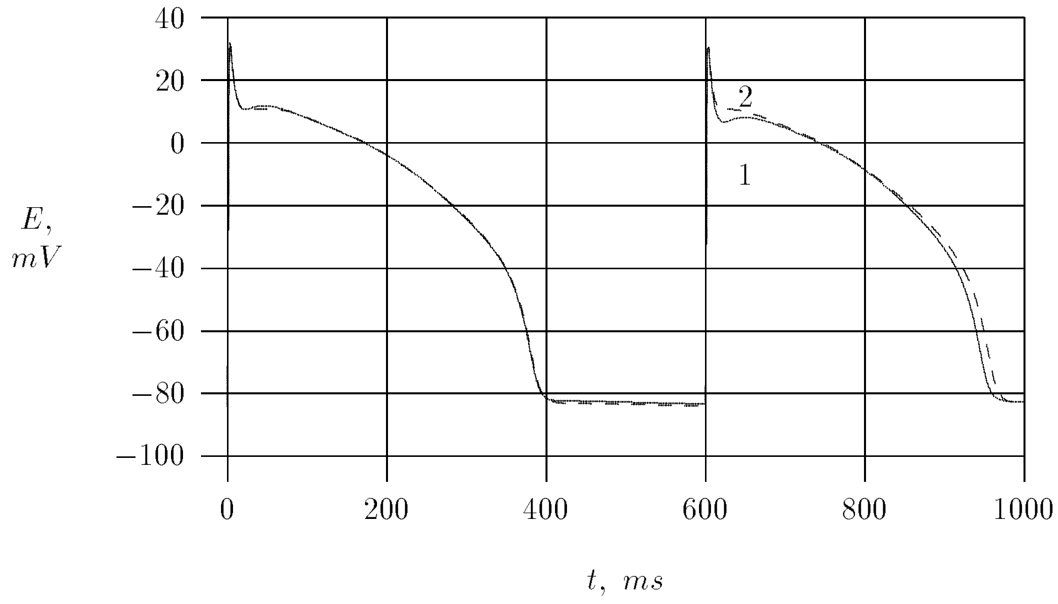


Figure 4.11: The shape of AP in case of repeatable excitation for the LR model (1) and for the third-order simplified model (2). $T_{stim} = 600ms$.

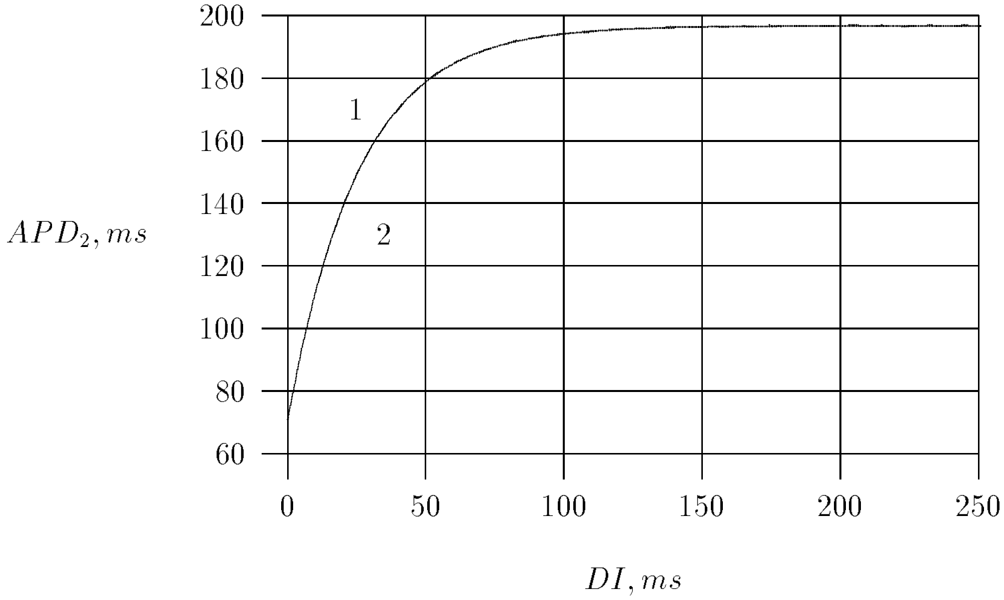


Figure 4.12: The APD restitution curve for the guinea pig heart (1) and its implementation in the third-order simplified model (2).

The $k_X(X_{init})$ table was constructed for the $200ms$ AP and APD restitution properties of the guinea pig heart [LGR94]. Figure 4.12 compares the original APD restitution curve with the one implemented in the model using the above approach. The difference between curves is very small, which proves the robustness of the proposed method.

When studying AP propagation, it is important to be able to consider independently the effects of APD and $(dE/dt)_{max}$ restitutions. It is possible to eliminate the APD restitution by selecting a very small time constant for $X$ immediately after repolarization. Similar thing can be done for $j$ to eliminate $(dE/dt)_{max}$ restitution (see chapter 5 for details).

## 4.3 Automatic Table Generation

To speed up the computation, the third-order simplified model uses tables instead of some complex non-linear functions participating in depolarization and repolarization currents. The drawback of the use of tables is that they have to be recreated every time the parameters of the model have changed. To minimize the inconvenience related to this problem an algorithm was developed to generate the tables automatically. This algorithm deals with the table of functions contributing to the currents in the model, which includes $fmmh(E)$, $X_i(E)$, $(I_{si} + I_l + I_{K1} + I_{Kp})(E)$, $\tau_j(E)$, $j_\infty(E)$, $\tau_x(E)$, $x_\infty(E)$. The algorithm uses the original LR model for computation and consists of two stages. At the first stage we simulate one AP using given parameters of the model. During every time step of this simulation all interesting functions are being saved in the large array in memory. On the next stage the range of change of $E$ is divided by the number of points in the table, therefore producing the table step. Then, for each of the values of $E$ in the table, the corresponding values of functions are picked out of the simulation results using interpolation, where necessary. The resulting table is later read by the third-order simplified model, which uses the nearest table value to compute its functions. Experiments showed that this approach with a table step as high as $1mV$ produced satisfactory results.

Another algorithm was developed to automate the creation of the $k_X(X_{init})$ table based on a given table of APD restitution data ( $APD_2$ vs. $DI$ ). Since the restitution property of the model is a result of its complex recovery processes, there is no way to compute $k_X(X_{init})$ directly, and we have to apply iterative numerical techniques to do that. The algorithm steps through all points of given APD restitution data and for each of them simulates two APs with the given $DI$ between them using fixed initial value of $k_X$. If the computed $APD_2$ differs from the required one, $k_X$ is adjusted and the simulation is repeated for the same $DI$. This is done until the difference between computed and given $APD_2$ is within 0.5 $mV$. After that, the $k_X$ and the corresponding $X_{init}$ are recorded in the table, and the process is repeated for the next APD restitution point. The adjustment rule for $k_X$ is as follows:

$$k_{X_{i+1}} = \begin{cases} k_{X_i} + 0.5|k_{X_i} - k_{X_{i-1}}| & \text{if computed } APD_2 > \text{given } APD_2 \\ \\ k_{X_i} - 0.5|k_{X_i} - k_{X_{i-1}}| & \text{if computed } APD_2 < \text{given } APD_2 \end{cases} \tag{4.19}$$

For the restitution curves we studied, $k_{X_0} = 0.7$ and $k_{X_1} = 1.0$ worked well. Experiments showed that the process converges within 10 iterations and allows us to simulate an APD restitution curve of any shape.

## 4.4 Conclusion

- A new methodology is developed for the synthesis of simplified models for propagation studies. This methodology can be applied to any full physiological model.

- The developed simplified third-order model based on the LR full physiological model correctly reproduces the cell recovery processes (including $(dE/dt)_{max}$ restitution) and the shape of AP.

- In the generation of one AP the use of this model with tabulated functions gives a 95 % decrease of computation time in comparison with the LR model, and about a 35 % decrease in comparison with the Van Capelle and Durrer second-order model.

- Significant speedup can be achieved by using automatically generated tables instead of non-linear functions in the model.

- The implementation of the APD restitution using the $k_X(X_{init})$ table provides great flexibility. For given $APD_2(DI)$ restitution data the proposed algorithm allows us to create this table automatically.

# CHAPTER 5

# Action Potential Propagation in a Ring of Cells

## 5.1 Introduction

The propagation of AP along a ring of cardiac cells is comparatively well studied phenomena. In physiological experiments [FS88], computer simulations and theoretical investigations [CGK93, KLZ94, Zyk87] it was shown that:

1. The stationary propagation of AP (with constant APD and $DI$) is possible when the slope of the APD restitution curve is smaller than 1 for the whole range of $DI$s and the length of the ring is greater than some critical value. When the ring length reaches the critical value, further propagation becomes impossible.

2. The stationary propagation may be transformed into stationary quasi-periodic oscillations (of APD, $DI$ and propagation velocity $\Theta$) by decreasing the ring length. That occurs when the slope of the APD restitution curve is equal to, or greater than 1 for at least one value of the $DI$.

3. The further shortening of the ring length leads to the unstable periodic oscillation and a breakup of the propagation.

The main objective of this chapter is to compare the AP propagation in the ring composed of cardiac cells described by the original LR mathematical model and the third-order simplified model, and to study the effect of the shape of the APD restitution curve on the character of AP propagation in the ring.

## 5.2 Mathematical Model and its Implementation

**General considerations** One-dimensional propagation of the AP is a particular case of the more general 3D propagation described by (4.2). Letting $y = z = 0$ we have:

$$-C\frac{\partial E}{\partial t} = I_{dep} + I_{rep} + I_{stim} + \alpha_x \frac{\partial^2 E}{\partial x^2} \tag{5.1}$$

Here, the expressions for the depolarization and repolarization currents are taken for the third-order simplified point model (see (4.11),(4.12)). The initial and boundary conditions are

$$E(x,0) = E_{rest}, X(x,0) = X_0, j(x,0) = j_0 \tag{5.2}$$

$$\left.\tfrac{dE}{dx}\right|_{x=x_B} = 0 \ - \quad \text{for the line of cells} \tag{5.3}$$

$$first\ and\ last\ nodes\ are\ considered\ neighbors - \ \text{for the ring of cells} \tag{5.4}$$

The one-dimensional line consists of a number of equidistant cells (nodes) interconnected by diffusion (5.1). Some time after the stimulus is applied to one of the ends of the line, both ends are connected numerically into a ring so that the first and the last nodes of the ring become neighboring nodes.

The main purpose of the ring simulations is to study the effect of the ring length on AP propagation. There exist two approaches to the variation of the ring length during simulation – one with the variable space step, the other with the fixed space step. According to the first approach, the space step is varied, leaving the number of the simulation nodes constant. This approach has three drawbacks:

- when using explicit numerical methods, the numerical stability determines a lower limit on the space step variation
- the minimal distance between cells in the real tissue imposes another lower limit on the space step variation
- large space step leads to the high resistance between nodes with the following propagation failure, which places an upper limit on the space step variation.

The second approach can be realized in two ways. One way is to start a new simulation with the open ring at each ring length. The second way is to start with the open ring at the initial ring length and then decrease the ring length continuously without interrupting simulation. The first way requires more time for simulation and leads to a larger critical length of the ring when propagation fails. Therefore, we used the second way in our simulations.

## 5.3 Effect of Passive Currents on the Shape of Propagating AP

Experiments show that the shape of the AP changes during 1D propagation. The change is most noticeable at the moment of cell excitation. This phenomenon can be explained by the influence of passive currents between cells. Figure 5.1 shows the front of AP and $I_n = \alpha_x \frac{\partial^2 E}{\partial x^2}$ in three consecutive points of the ring during wave propagation in the ring with the initial conditions corresponding to the rest state. The AP reaches its peak at 22.9, 23.5, 24.1 $ms$ in the node 1, 2

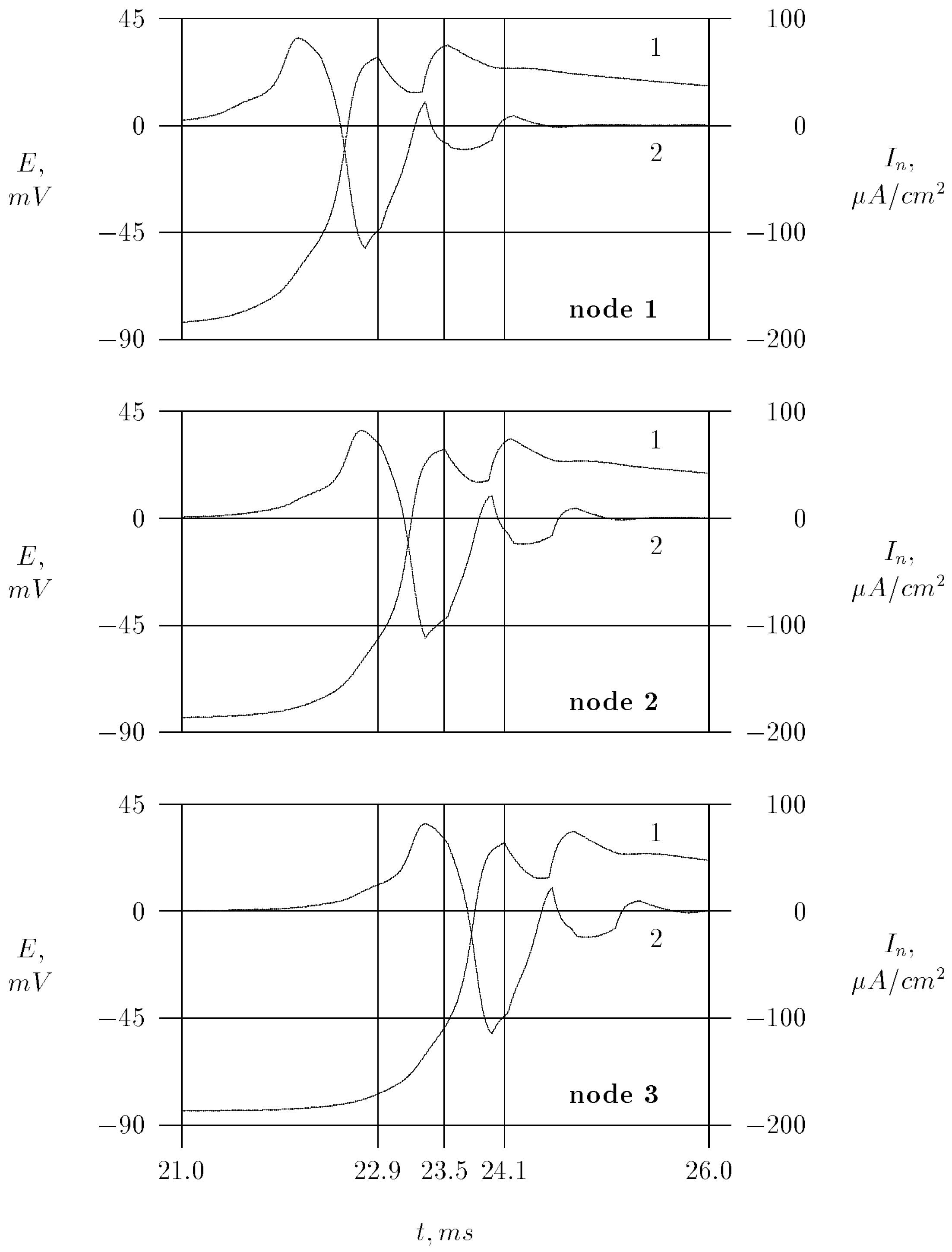


Figure 5.1: The front of AP (1) and $I_n$ (2) in three consecutive points of the ring during wave propagation. The initial conditions correspond to the rest state.

and 3 respectively. Let us consider the excitation of the cell in these conditions using node 2 as an example. The excitation starts when the large positive $I_n$ appears as a result of node 1 excitation. It drives the voltage above the threshold and causes the excitation of the cell. Since the voltage difference between nodes 1 and 2 becomes small, $I_n$ drops to 0. At this moment, however, the difference in voltage between nodes 2 and 3 becomes very big, which produces large negative $I_n$ in the node 2, which, in turn, prevents the AP from growing further up to its natural maximum. As a result we see a dip in the upper part of the front. About 0.3 $ms$ later the AP in the node 3 becomes large enough, so the $I_n$ in the node 2 becomes small again, and AP in the node 2 gets a chance to grow a little bit more before switching to the repolarization phase. The excitations of nodes 4 and 5 (not shown) produce a few more oscillations of $I_n$ and AP, which are negligible. During the repolarization phase of the AP the passive currents are very small, therefore, the shape of the AP is very close to that in a cell.

The effect of passive current changes when the wave propagates with the initial conditions different from the rest state. Figure 5.2 shows three consecutive nodes of the ring during the propagation of the premature beat with the $DI = 35ms$. Here, due to the effect of the $(dE/dt)_{max}$ restitution, $I_{Na}$ in the cell is lower and, therefore, the slope of the AP front is lower. At the same time, $I_K$ is higher because of the APD restitution. Both of these factors prevent the formation of the second peak on the front of AP. Since the effect of both restitutions depends on the $DI$, the resulting shape of the AP front will vary with $DI$.

The change in the AP front due to the passive currents doesn't change the APD for more than 0.5 $ms$ and hardly affects propagation in general.

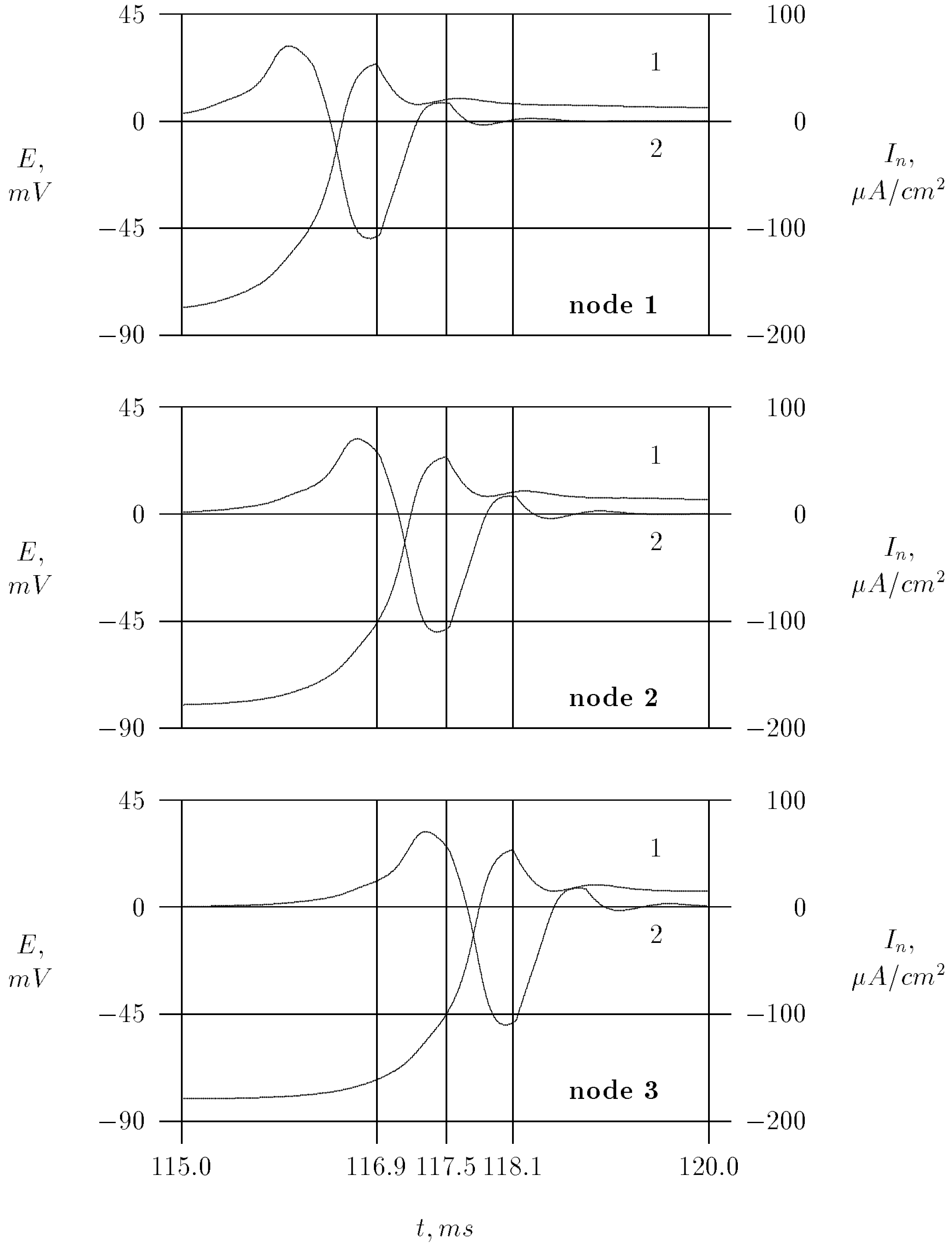


Figure 5.2: The front of AP (1) and $I_n$ (2) in three consecutive points of the ring during wave propagation. Premature stimuli, $DI = 35ms$.

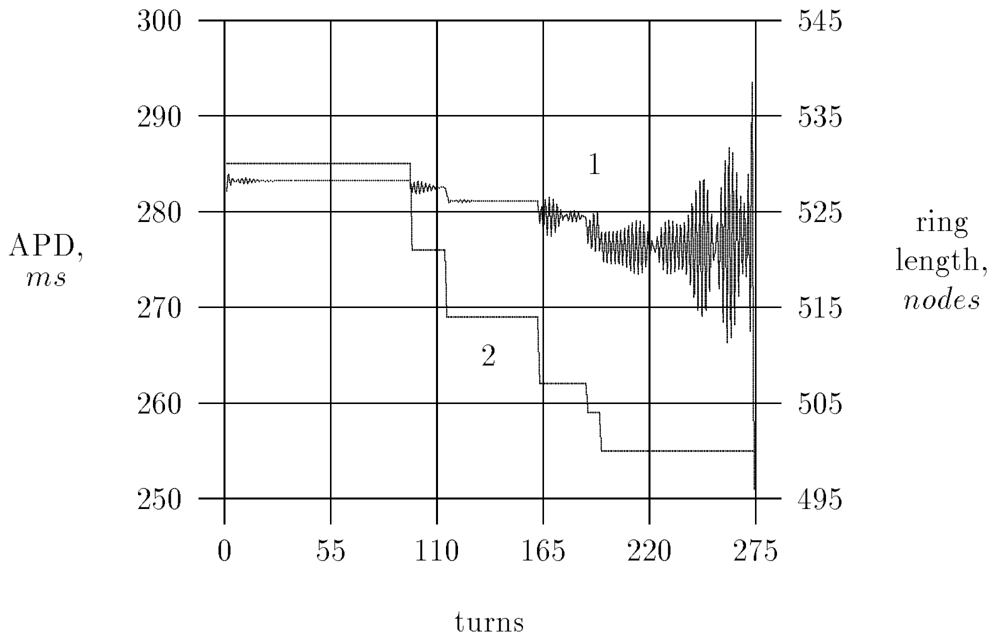


Figure 5.3: APD in a point of the ring during the consecutive ring shortening for the LR model. 1 – APD, 2 – ring length.

## 5.4 AP Propagation with the Original APD Restitution. Comparison with the LR Model

The developed third-order simplified model was created on the basis of the full LR I model [LR91], therefore it is worthwhile to compare the results of the wave propagation in a ring composed of the cells described by our simplified model and the cells described by the full LR model. This will give us further verification of the simplified model for 1D case.

The simulation with the LR model was done using original parameters. The APD and $(dE/dt)_{max}$ restitution curves for this model are given in Fig. 4.5. The restitution curve has a slope greater or equal to 1 only for very short $DI$s. The diffusion coefficient $\alpha_x$ is chosen equal to 0.0005 $m\Omega^{-1}$ to provide the speed of

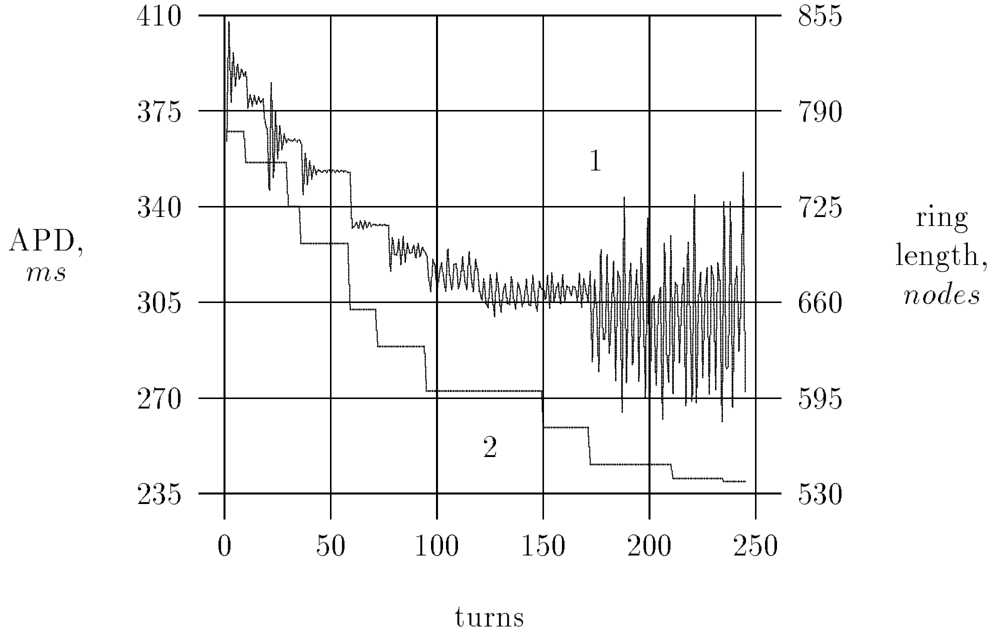


Figure 5.4: APD in a point of the ring during the consecutive ring shortening for the third-order model. 1 – APD, 2 – ring length.

propagation $40cm/s$. The distance between nodes is 0.02 $cm$.

For the simulation shown in Fig. 5.3, the initial number of nodes in the ring was 530. For the ring length 530 nodes the duration of the propagated AP after some transient period stabilizes around some steady state level. After consecutive shortening of the ring to 507 nodes the APD doesn't stabilize any more and continues to oscillate with comparatively small amplitude. Further decrease of the ring length produces an increase in the oscillations amplitude. At the length of 500 nodes the amplitude rapidly increases until the propagation stops.

Qualitatively the same behavior is observed in the third-order simplified model (see Fig. 5.4). The protocol of ring shortening determines the critical length of the ring and APD at the moment of propagation breakup. The simulation in

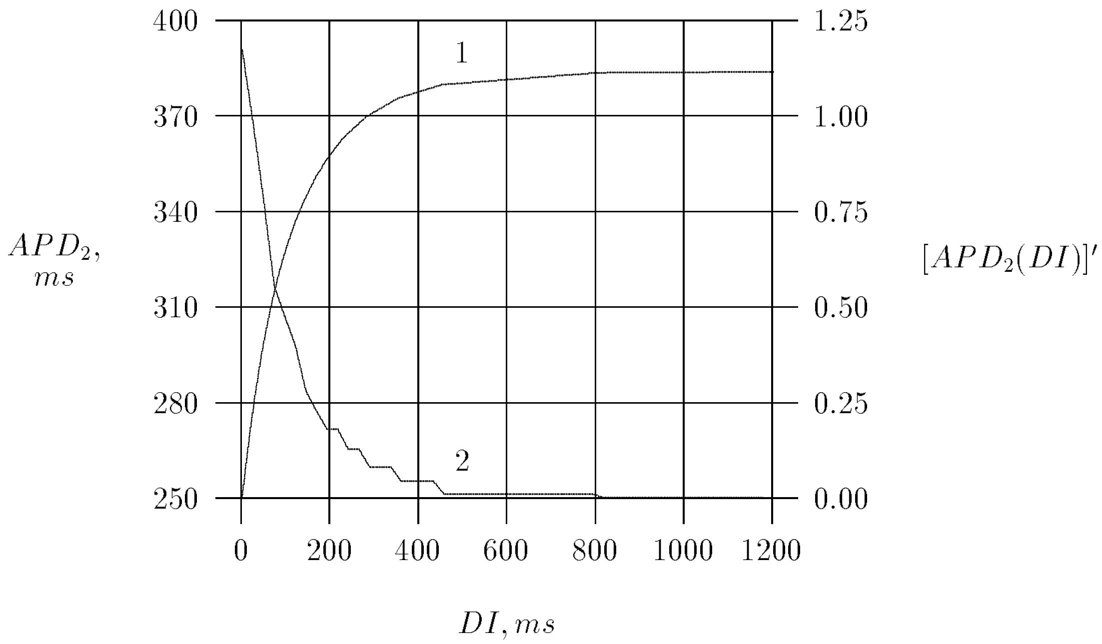


Figure 5.5: The modified APD restitution curve of the third-order model (1) and its derivative (2).

Fig.5.3 and Fig.5.4 were done using different protocols since the simulation with the LR model is much more time consuming. This explains the quantitative differences in the results.

## 5.5 Effect of the APD Restitution Slope Increase on the AP Propagation

The results shown in the previous paragraph are true when the slope of the APD restitution curve is equal to 1 only on a small range of $DI$s. It is of great importance to study how the slope of the restitution curve affects the propagation in the ring. For this purpose computer simulation was done when the original

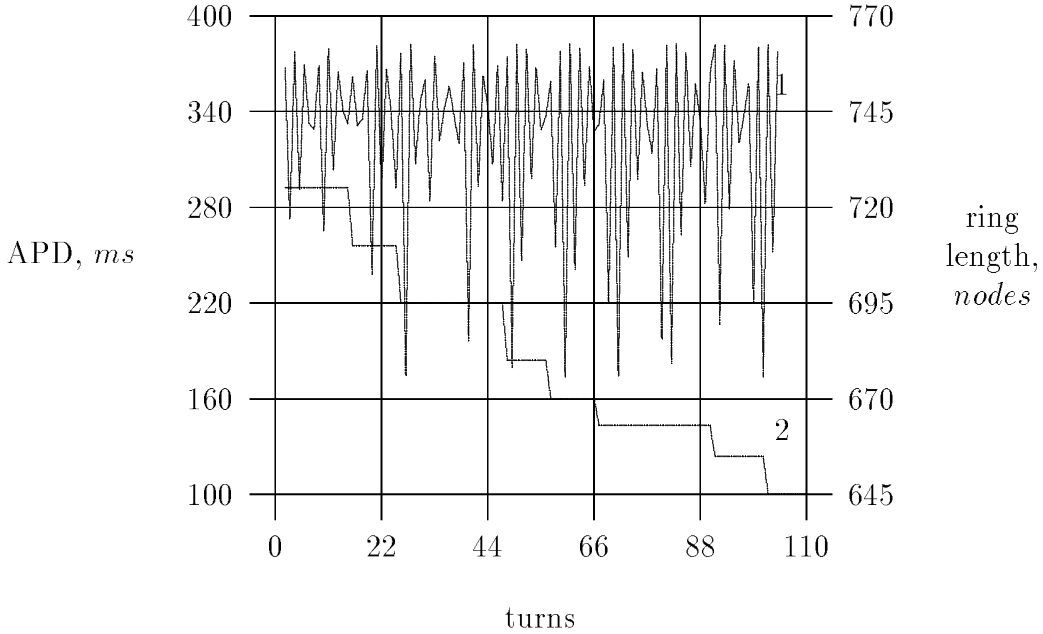


Figure 5.6: APD in a point of the ring during the consecutive ring shortening for the third-order model. 1 – APD, 2 – ring length.

restitution curve was modified as shown on Fig. 5.5. Here, the restitution curve has a slope greater or equal to 1 in the range of $DI$s from 0 to 50 $ms$. This result was obtained using the same approach that was used in 4.18 for fitting the LR restitution curve. Namely, the time constant $\tau_x$ was changed according to the following rule

$$\tau_X^*(E) = \begin{cases} 1.0\tau_X(E) & \text{if } dX/dt \geq 0 \\ 0.002\tau_X(E) & \text{if } dX/dt < 0, X \geq 0.26 \\ 0.15\tau_X(E) & \text{otherwise} \end{cases} \tag{5.5}$$

Fig. 5.6 shows the dependence of the APD in one point of the ring on the number of turns of the wave during the successive shortening of the ring length. Comparison with Fig. 5.4 shows that at the same ring length, instead of stationary propagation, the instability occurs which is expressed in increasing oscillation of the APD with the shortening of the ring length. Starting with the ring length 680 nodes one can observe quasi-periodic behavior of the APD oscillations. The wave propagation blocks after 140 turns at the ring length of 645 nodes.

There exists a critical length of the ring for which the AP propagation becomes impossible. When the slope of the APD restitution curve is smaller than 1, for our model $L_{cr} = 10.76\ cm$. When the slope of the APD restitution is greater than 1 for some diastolic interval, there exists a range of ring lengths (in our case $12.9\ cm < L < 13.9\ cm$) where propagation of AP is unstable. For greater ring lengths the AP circulating in the ring reaches its steady state duration and velocity of circulation. The lower limit of the range of instability corresponds to the critical ring length when AP no longer can propagate. This coincides with theoretical results and computer studies done for the Beeler – Reuter mathematical model [KLZ94, CGK93].

## 5.6 Propagation of the Short AP with the Steep APD Restitution Curve

It is known from physiological experiments, that when the cardiac tissue is affected by cromakalim, the AP changes its shape and duration [SSZ88]. In 2D tissue under these conditions the spiral wave activity is developed. To be able to simulate the AP propagation in one- and two-dimensional tissue under these conditions the parameters of AP in the model have to be adjusted. For this purpose, we changed the APD of the LR model by increasing two components of

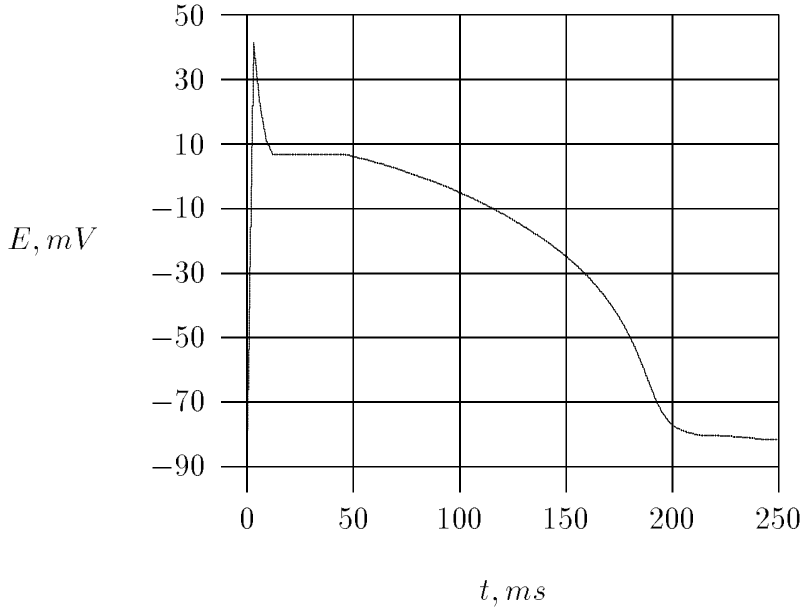


Figure 5.7: Shortened AP. $APD = 196ms$.

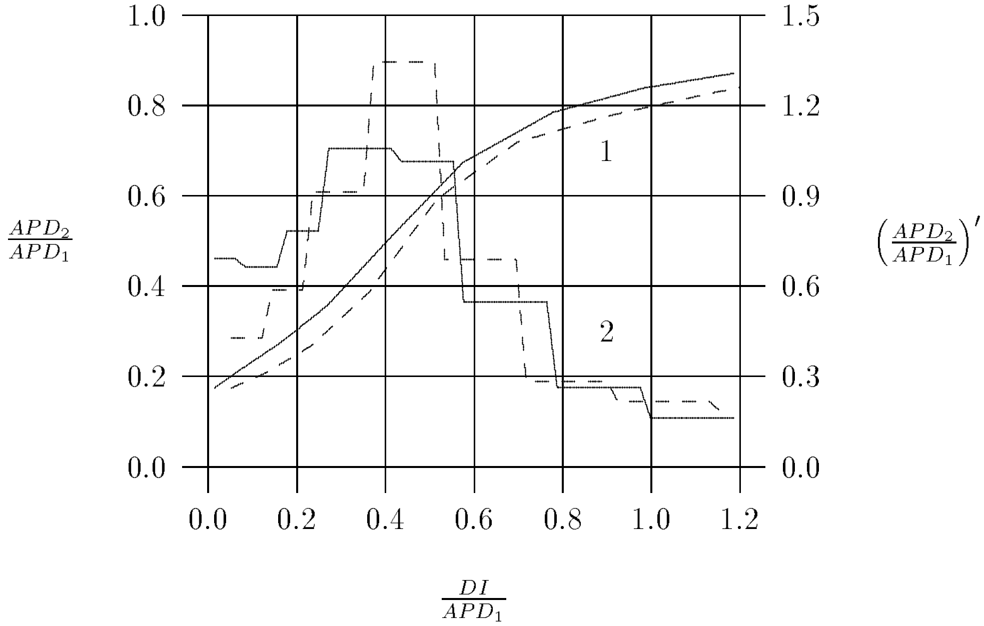


Figure 5.8: The APD restitution curves (1) for the LR model and the third-order model with the short AP, and their derivatives (2). LR model – solid lines, third-order model – dashed lines.

potassium current, namely by increasing $I_K$ 6 times, and by increasing the rest of the repolarization currents 1.7 times. Fig. 5.7 shows the resulting AP, and Fig. 5.8 shows the resulting APD restitution curve. The APD restitution curve is $S$-shaped and has a slope greater than 1 in the range of $DI$s from 30 to 55 $ms$. Using method described in chapter 4 the function tables were generated for use in the simplified third-order model. In order to obtain in the simplified model the same APD restitution curve, the APD restitution table was generated (see section 4.3 and Fig. 5.8).

The results of the ring simulation (recorded in one point of the ring) with the successive ring shortening are given in Fig. 5.9. For ring lengths higher than 450 nodes ($9cm$) the propagation reaches steady-state condition. For the shorter ring lengths up to 150 nodes ($3cm$) the instability in APD occurs. Further shortening leads to another stable region which ends at approximately 60 nodes ($1.2cm$) when propagation fails. The region of maximum amplitude of APD oscillations corresponds to the ring length of 270 nodes ($5.4cm$). Fig. 5.10 shows the oscillations of APD for that ring length. The oscillations are quasi-periodic with the period of slow modulation equal to 37 turns and the period of fast oscillations equal to 3 turns. The maximum amplitude of APD oscillations is about 90 $ms$, but at the same time the maximum amplitude of cycle length oscillations does not exceed 10 $ms$.

The third-order simplified model is distinguished from the other simplified models by the fact that it reproduces $(dE/dt)_{max}$ restitution. To study the effect of the $(dE/dt)_{max}$ restitution on the propagation in the ring, the above experiment was repeated without the $(dE/dt)_{max}$ restitution. This was achieved by changing

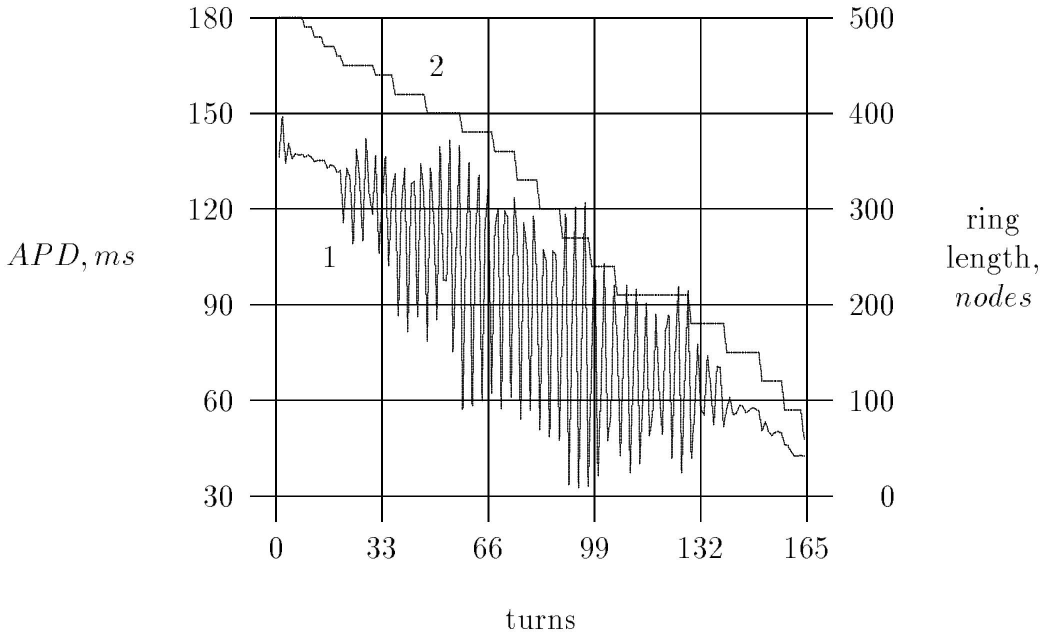


Figure 5.9: The consecutive ring shortening for the third-order model with the steep restitution curve with $j$. 1 – APD, 2 – ring length.

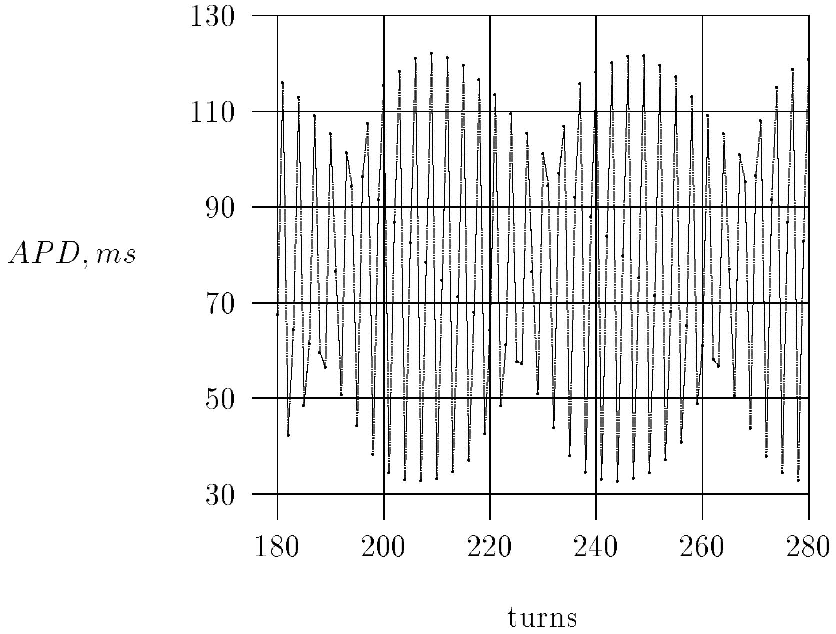


Figure 5.10: APD oscillations with $j$ present. Ring length 270 nodes.

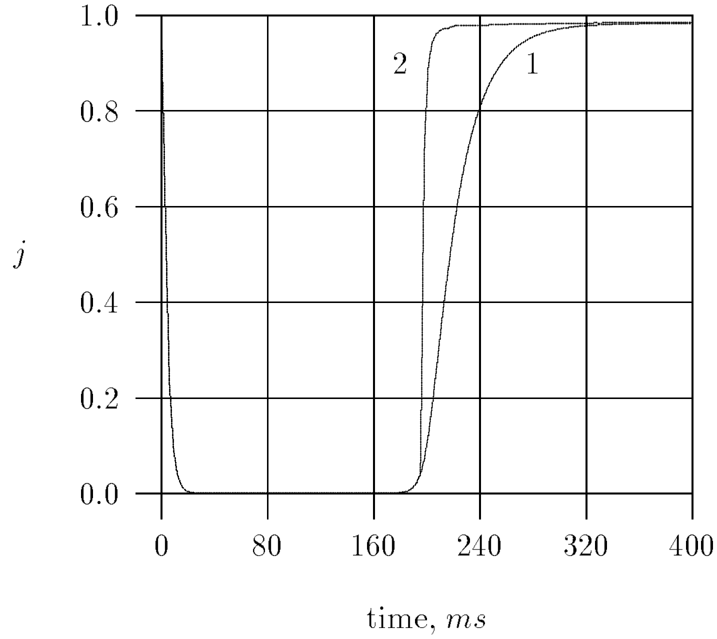


Figure 5.11: Original (1) and modified (2) $j(t)$.

the time constant of gate variable $j$ in the following manner:

$$\tau_j^*(E) = \begin{cases} 1.0 & \text{if } dE/dt < 0 \text{ and } E < -70 \\ \\ \tau_j(E) & \text{otherwise} \end{cases} \tag{5.6}$$

The time course of $j$ with the original and modified $\tau_j$ is presented in Fig. 5.11.

The results of the simulation with the successive ring shortening are given in Fig. 5.12. For ring lengths higher than 450 nodes ($9cm$) the propagation reaches steady-state condition. For shorter ring lengths, from 180 to 450 nodes ($3.6cm$), the instability in APD occurs. Further shortening leads to another stable region which ends at approximately 90 nodes ($1.8cm$) when propagation fails. The region of maximum amplitude of APD oscillations corresponds to the ring length of 270 nodes ($5.4cm$). Fig. 5.13 shows the oscillations of APD for the

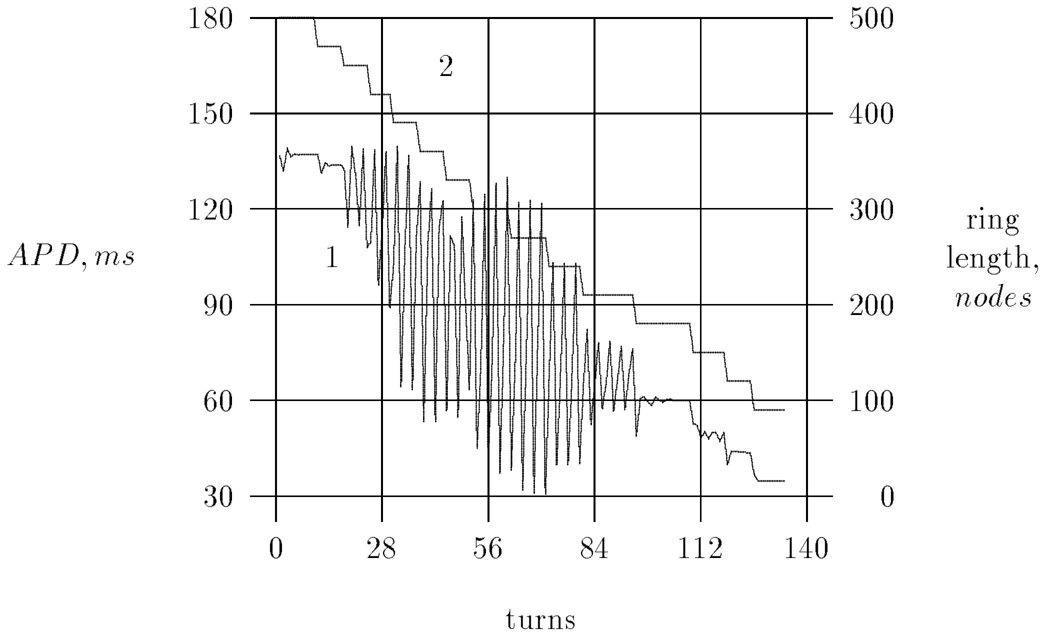


Figure 5.12: The consecutive ring shortening for the third-order model with the steep restitution curve without $j$. 1 – APD, 2 – ring length.

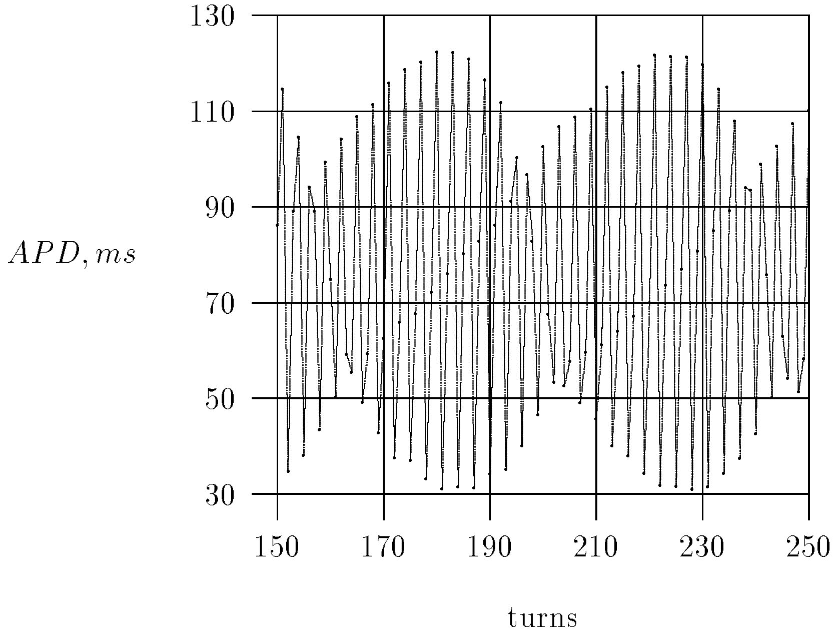


Figure 5.13: APD oscillations without $j$ present. Ring length 270 nodes.

ring length of 270 nodes. The oscillations are quasi-periodic with the period of slow modulation equal to 40 turns and the period of fast oscillations equal to 3 turns. The maximum amplitude of APD oscillations is about 90 $ms$, but at the same time the maximum amplitude of cycle length oscillations does not exceed 3 $ms$.

The difference in the behavior of the system with $j$ and without $j$ can be explained as follows:

- The instability in both cases starts at about the same ring length due to the fact that for this ring length the $DI$ is relatively big. $j$ is expressed significantly only at short $DI$s and, in this case doesn't affect propagation.
- The range of the ring lengths where the instability can be observed is larger for the case with $j$. This can be explained by the fact that $j$ reduces the propagation velocity and destabilizes the process for the short $DI$s.
- The reduction of the propagation speed by $j$ causes the decrease of the wave length of propagated pulse and allows the AP to exist in shorter rings.

## 5.7 AP Propagation with Monotonic APD Restitution Curve

It was found that the APD restitution curve for the cardiac cell of the guinea pig heart is monotonic [LGR94] (see Fig. 5.14, curve 1). The maximum APD corresponding to this curve is 192 $ms$. To be able to use it with the simplified model, which has APD 196 $ms$, the curve was adjusted to 196 $ms$ (see Fig. 5.14, curve 2). The simulation with this restitution curve allows us to compare the

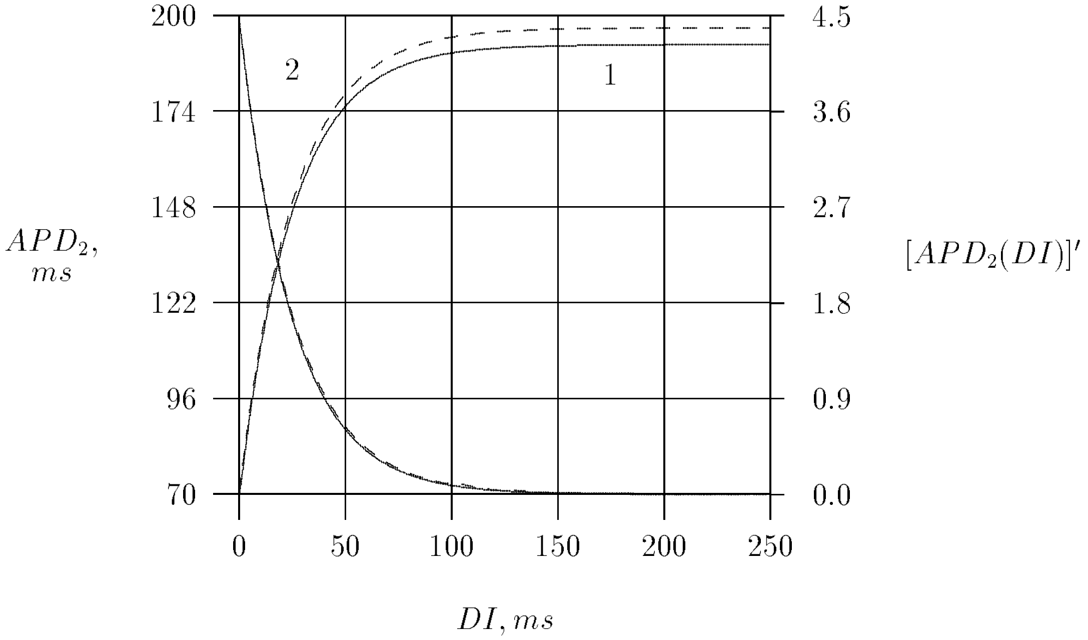


Figure 5.14: The guinea pig APD restitution curve (1) and it's derivative (2). original – solid lines, adjusted – dashed lines.

propagation with different restitution curves. The slope of this restitution curve is higher than 1 for $DI$s less than 40 $ms$.

The experiments were conducted for three ring lengths 500 (10 $cm$), 420 (8.4 $cm$) and 350 (7 $cm$) nodes which correspond to the beginning of the instability range, the middle of the instability range and the vicinity of the break up point. For ring lengths larger than 500 nodes the APD oscillations converge to the steady-state value. The simulation with the 500 node ring (Fig. 5.15) shows a small range of APD oscillations (10 $ms$) with a very large period of modulation (approximately 787 turns). The APD is distributed periodically along the ring (see Fig. 5.16) and the period of this distribution (999 nodes) is slightly less than two ring lengths (1000 nodes). This slight difference leads to the modulation of

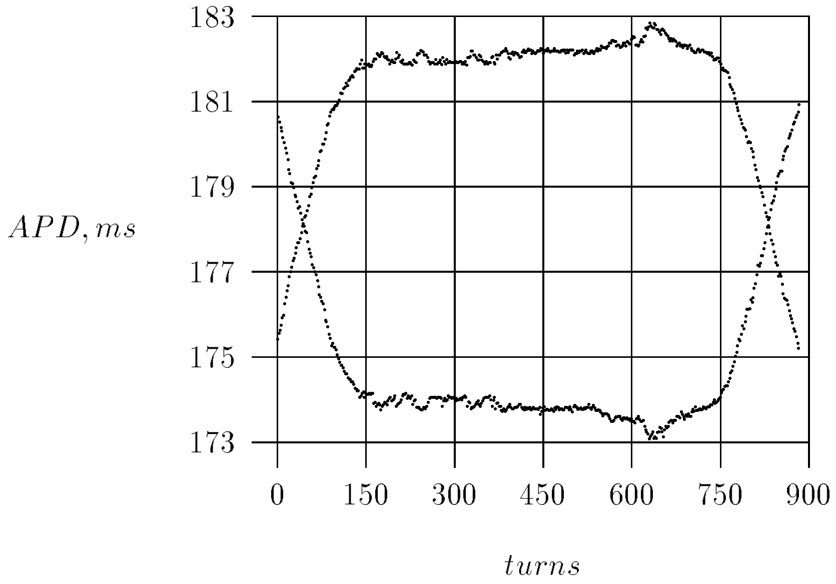


Figure 5.15: APD recorded in one point of the 500 node ring. High frequency oscillations are not shown.

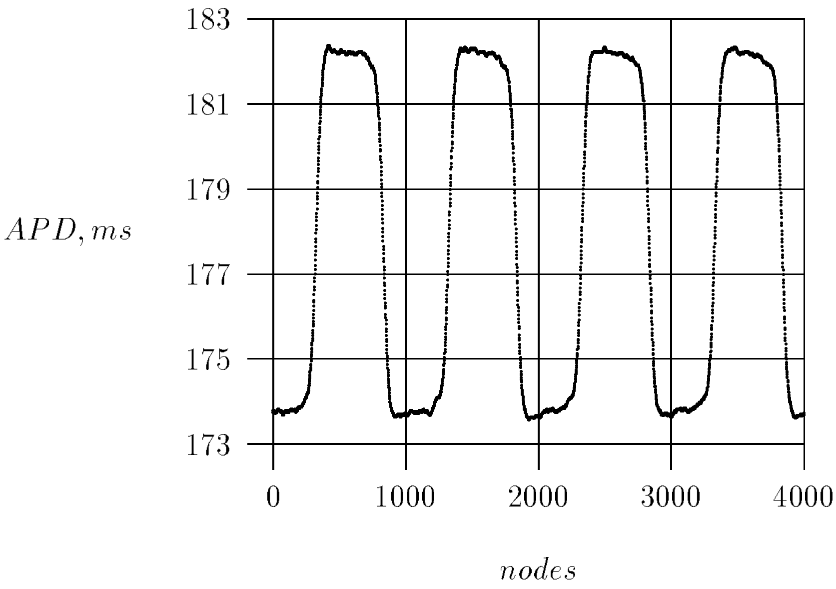


Figure 5.16: APD distribution along the 500 node ring during 8 turns of the wave.

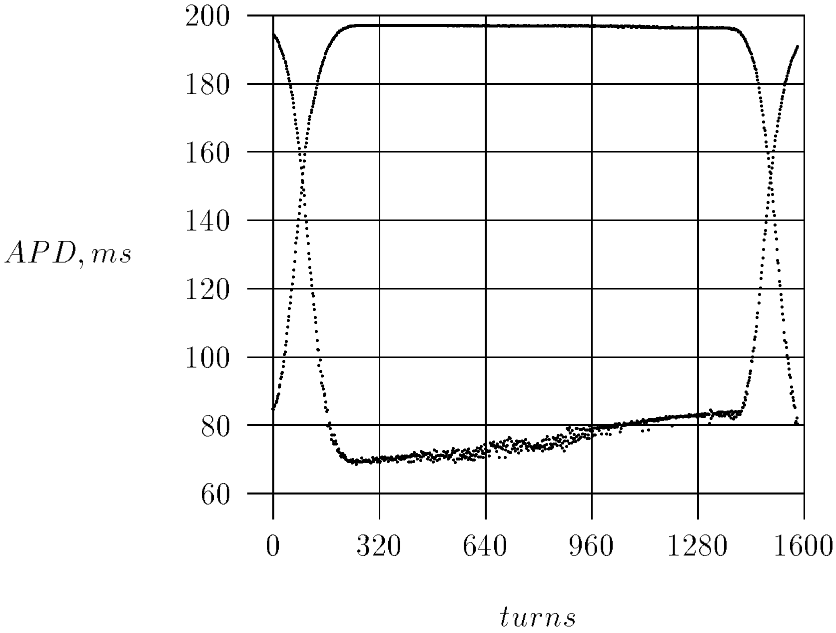


Figure 5.17: APD recorded in one point of the 420 node ring. High frequency oscillations are not shown.

APD oscillations observed in one node of the ring. The smaller the difference, the larger the period of modulation. The period of modulation, therefore, can be estimated as

$$\frac{2L}{2L - \lambda} \tag{5.7}$$

where $L$ is the ring length and $\lambda$ is the period of spatial APD distribution. The use of this formula requires very precise measurement of $\lambda$ during a large number of periods. Otherwise, it produces significant error. The cycle length changes insignificantly as does the average speed of propagation.

After shortening the ring length to 420 nodes we obtained the pronounced oscillations of APD and $DI$. APD in one point of the ring is presented in Fig. 5.17. The range of APD oscillations is 134 $ms$ and the period of slow modulation is

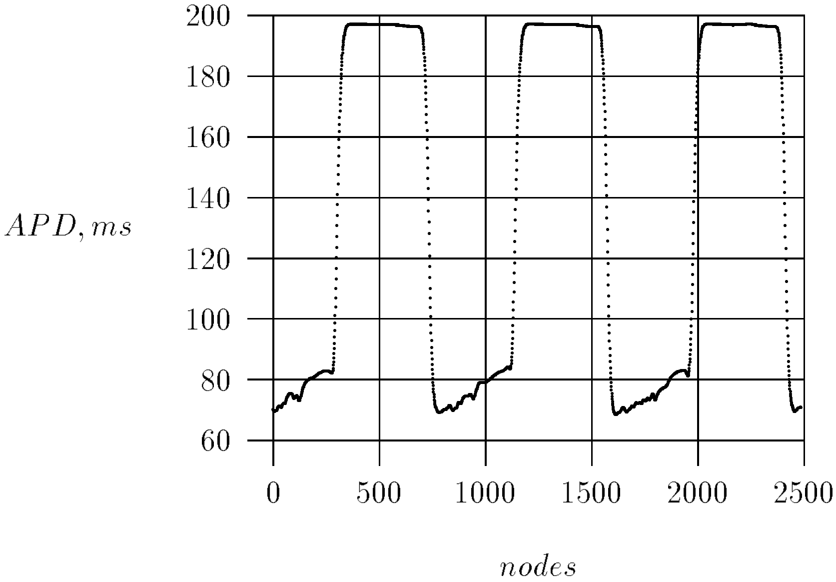


Figure 5.18: APD distribution along the 420 node ring during 8 turns of the wave.

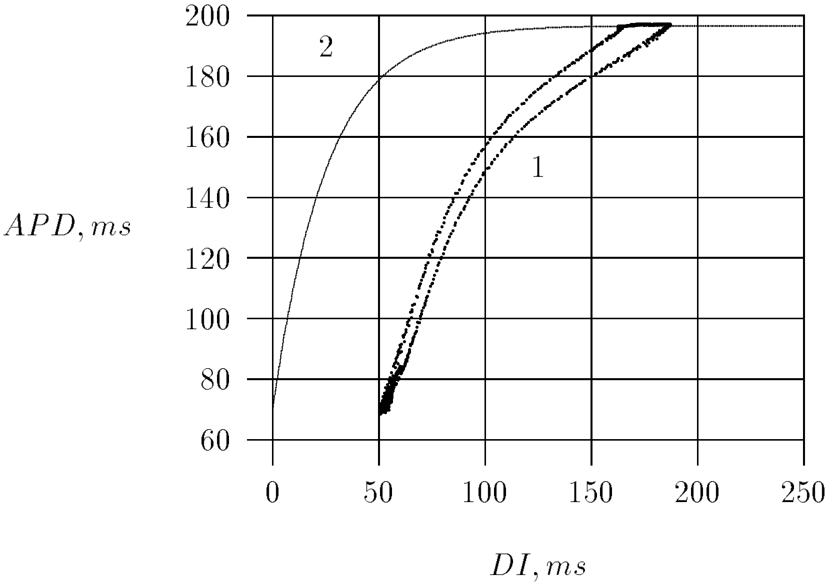


Figure 5.19: The dynamic APD restitution curve for the 420 node ring (1) along with the static APD restitution curve (2).

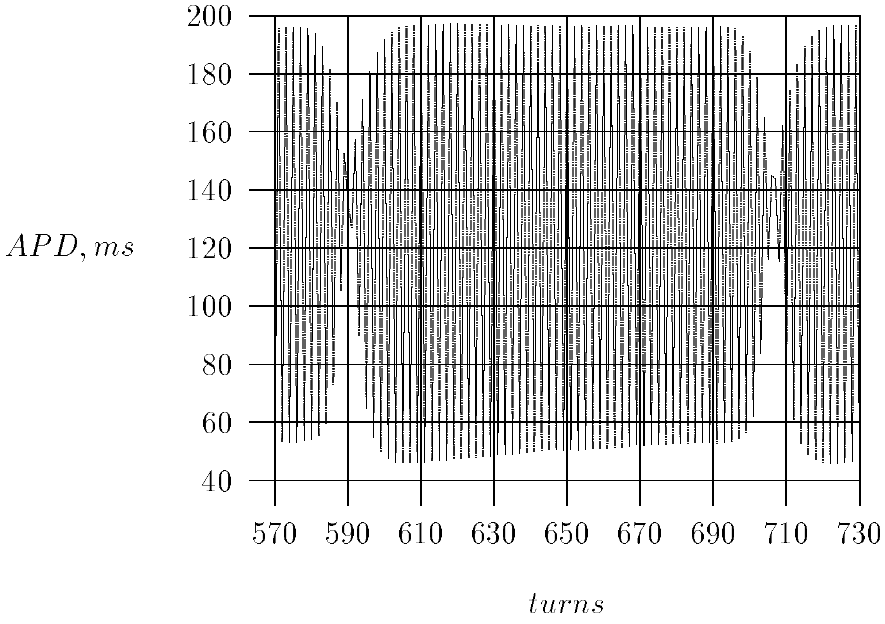


Figure 5.20: APD recorded in one point of the 350 node ring.

about 610 turns. The range of the cycle length variation is about 25 $ms$. The spatial distribution of APD is shown in Fig. 5.18. The period of this distribution is 838, which is smaller than 2 ring lengths by 2. The dependence of the APD on the previous $DI$ obtained during this simulation is shown in Fig. 5.19. This curve is no more a single-valued function of $DI$. The difference between upper and lower branches of this curve is between 5 and 10% depending on the value of $DI$. The multivaluedness of this curve can be explained by the fact that the APD restitution curve in a cell depends on the history of previous excitations. Since during the unstable propagation a cell goes through different excitation scenarios the dependence we obtain is a composition of parts of different restitution curves. This must be taken into consideration when comparing the results obtained using the theoretical approach proposed in [CGK93] with the results of simulation and electrophysiological experiments of ring propagation.

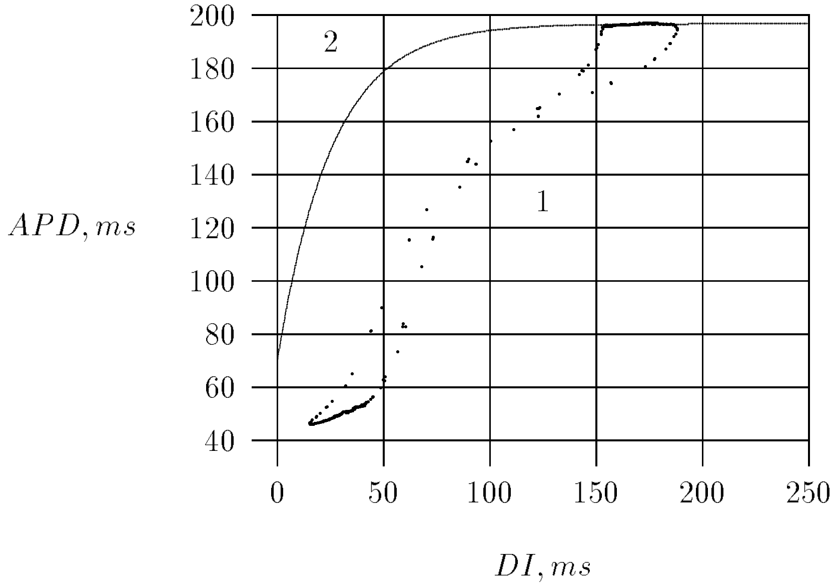


Figure 5.21: The dynamic APD restitution curve for the 350 node ring (1) along with the static APD restitution curve (2).

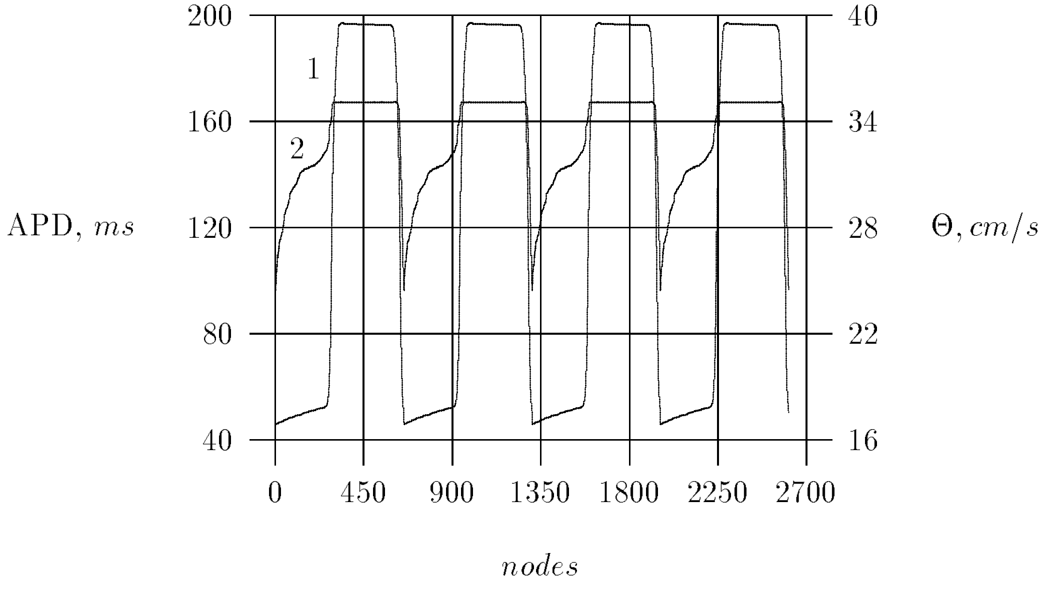


Figure 5.22: Distribution of the APD (1) and the propagation velocity (2) along the 350 node ring during 8 turns of the wave. The node 0 corresponds to the end of the transient period.

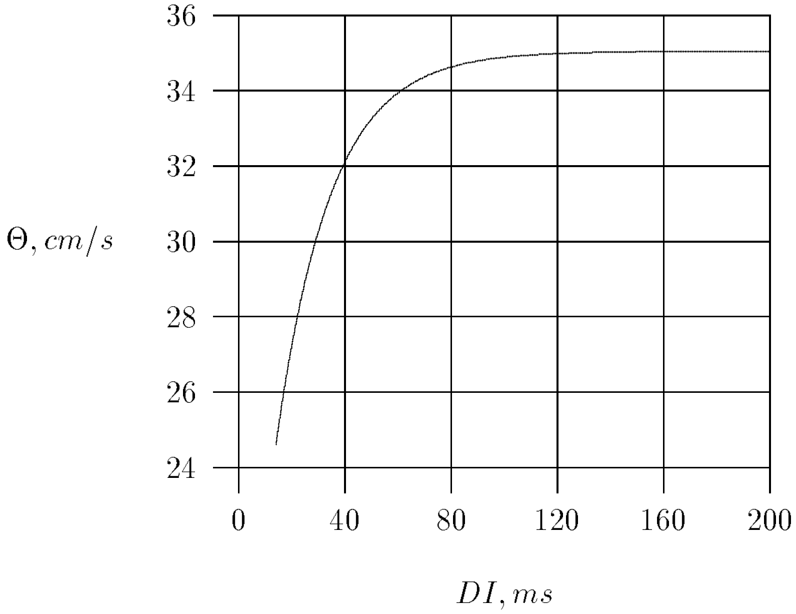


Figure 5.23: The dispersion curve for the 350 node ring

In case of the 350 node ring the range of oscillations has further increased to 150$ms$ (see Fig. 5.20). The modulation period is approximately 116 turns. The amplitude of oscillations is so big that the APD reaches its maximum values in the middle of the slow modulation period. The range of the cycle length variation is about 35 $ms$. The dependence of the APD on the previous $DI$ obtained during this simulation is shown in Fig. 5.21. The difference between upper and lower branches of this curve is between 3 and 25% depending on the value of $DI$. The spatial distribution of APD is shown in Fig. 5.22. The period of this distribution is about 652 nodes, which is smaller than 2 ring lengths by 48 nodes. The dependence of the wave speed on the $DI$ (dispersion curve) is presented in Fig. 5.23.

## 5.8 Conclusion

The computer simulation of the AP propagation in the ring of cardiac cells with the third-order simplified model shows that

- The propagation in the ring is qualitatively the same as with the full LR I model. This proves that the third-order simplified model can be used for computer simulation of 1D propagation.
- The introduction of the $(dE/dt)_{max}$ restitution increases the range of the ring lengths where the instability is observed.
- The slope of the APD restitution curve plays a crucial role in the character of AP propagation, namely it determines the appearance of APD quasi-periodic oscillations in the ring, the amplitude of these oscillations, and the ring length for which the wave breakup occurs.
- The APD restitution measured during the quasi-periodic oscillations is a two-valued function with the difference between values up to 25% for the 350 node ring. With the increase of the ring length the difference between values diminishes. The dynamic APD restitution curve is located under the static APD restitution curve (see Fig. 5.19 and Fig. 5.21).
- The shape of the AP upstroke changes slightly during propagation due to the effect of local currents from neighboring cells.
- When the propagation in the ring exhibits quasi-periodic oscillations the APD distribution along the ring is periodic with the period $\lambda$ smaller than 2 ring lengths. The shape of this distribution depends on the APD restitution

curve. The period of slow modulated oscillations can be determined as $T = 2L/(2L - \lambda)$.

# CHAPTER 6

# Action Potential Propagation in the Uniform 2D Tissue

## 6.1 Introduction

In the past, the simulations of AP propagation in 2D tissue were mainly done using the simplified second-order cell models. Many interesting properties of this propagation were found including stationary and nonstationary spiral wave formation [GP72, PDS93, Win89, KKB93] and the appearance of the spiral wave breakup [Kar94]. It is of great interest to simulate the same phenomena using the third-order simplified model. Unfortunately, the results obtained in 1D simulations can not be immediately applied to the propagation in 2D. However, the previous investigations have shown that the APD restitution [KKB91b] and $(dE/dt)_{max}$ restitution [KKK95b] play a crucial role in spiral wave propagation.

The computer simulations were done using the massively parallel computer CM-2 and the 270 MHz DEC Alpha serial workstation.

## 6.2 Features of the CM–2

The version of CM–2 we used consists of 16K processors and provides two types of interprocessor communications. The NEWS (north, east, west, south) grid is a two - dimensional scheme which permits each processor to communicate with its nearest neighbor directly. Processors may also communicate via a 12 dimensional hypercube topology. Each processing element contains a very simple 1-bit arithmetic and logic unit (ALU) and 64K bits of local memory. In addition, each processing element has four 1-bit flag registers, an I/O interface, and shares an optional floating point accelerator (among 32 processing elements).

Operation on the CM-2 is in single instruction multiple data (SIMD) stream mode. During execution, the front-end computer(s) sends a stream of high level instructions to sequencers which in turn convert these to microcode instructions (nanoinstructions). These nanoinstructions are broadcast to the individual processing elements and control their timing and operations.

Data level parallelism uses a single control sequence or program, where code is executed sequentially. All programs are stored in the front-end computer. Note that the processor memory contains only data and immediate computations, and does not contain code for execution.

In situations where the number of physical processors is not enough to adequately meet the degree of data level parallelism, the CM-2 can support virtual processors.

The architecture of CM-2 corresponds very well to the 2D grid of nodes for the finite difference model of the heart muscle. The interprocessor communication system provides the minimum time for the interchange of data between the neighboring nodes of the simulation grid. This makes CM-2 a very effective tool for the simulation of wave propagation in heart muscle.

The main drawbacks of the CM-2 are:

- The size of the simulation grid is effectively limited by the number of CM-2 processors, since the use of virtual processors significantly slows down simulation.

- The small amount of memory in each node prevents the use of advanced numerical techniques, such as tabulation of functions.

- The choice of numerical method is limited to methods that require little interprocessor communication.

- The slow speed of node processors.

These drawbacks are non-existent in serial computers the power of which has grown tremendously during the last years. One of today's fastest serial workstations is 270 MHz DEC Alpha. We simulated $128 \times 128$ node problem on both CM-2 and DEC Alpha with the same computation time. The use of tables in the serial version of the program allowed us to reduce the computation time on DEC Alpha even more.

The $200 \times 200$ node simulations presented here were done using DEC Alpha workstation. The preliminary simulations with the $128 \times 128$ node grid were done on the CM-2.

## 6.3 Algorithm

The objective of our simulation is to find the distribution $E = f(x, y, t)$ in the heart muscle using the simplified third-order mathematical model. For the 2D case after the finite difference approximation of the Laplacian we obtain the following system of PDE

$$
\begin{aligned}
-C\frac{dE}{dt} &= I_{dep}(E,t) + I_{rep}(E,t) + I_{stim} + I_n && (6.1)\\
I_{dep}(E,t) &= j(E,t)f_1(E) && (6.2)\\
I_{rep}(E,t) &= f_2(E) + X(E,t)f_3(E) && (6.3)\\
\tau_j(E)\frac{dj}{dt} &= j_\infty(E) - j && (6.4)\\
\tau_X(E)\frac{dX}{dt} &= X_\infty(E) - X && (6.5)\\
I_n &= \frac{E_{(m-1)n}(t) - 2E_{mn}(t) + E_{(m+1)n}(t)}{\Delta x^2} + && (6.6)\\
&\quad \frac{E_{m(n-1)}(t) - 2E_{mn}(t) + E_{m(n+1)}(t)}{\Delta y^2}. && (6.7)
\end{aligned}
$$

The functions $f_1(E)$, $f_2(E)$ and $f_3(E)$ are described by (4.15) – (4.17). The initial distributions of $E_{mn}(0)$, $j_{mn}(0)$ and $X_{mn}(0)$ are specified. The boundary conditions are

$$\frac{\partial E}{\partial x} = 0 \quad and \quad \frac{\partial E}{\partial y} = 0 \tag{6.8}$$

In order to take advantage of the data level parallelism in the CM-2, the method of lines is chosen. Equations (6.1) – (6.7) are computed for each grid point during each integration time step. A slight variation of the method of lines (proposed in [GKR67] for implementation on hybrid computers and further developed in [Pet75]) is used to reduce the amount of communication between neighboring grid points. This is achieved by holding off the evaluation of the equation (6.7) to integral multiples of the integration time step. The choice of this interval is such that the interval is small enough for $I_n$ to be assumed constant over that interval. Several numerical methods are used for integration, including Euler, second order Runge-Kutta, and Ashour-Hanna [AH90]. For the Ashour-Hanna method the integration time step is $\Delta t = 0.025ms$ and parameter $\alpha = 0.76$, which provides the required accuracy and stability [KKB91a].

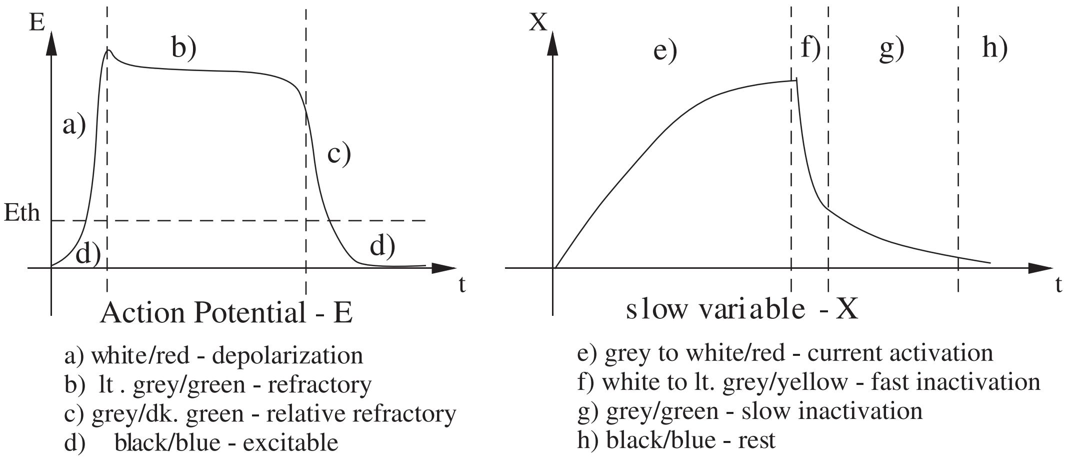


Figure 6.1: Schematic representation of color/grey level designations for action potential $E$ and slow gate variable $X$.

## 6.4 Graphical Representation of the Results

The results of simulation are presented in two color pictures displaying AP and the slow variable $X$. The pictures are updated every communication interval. The color coding is explained in Fig. 6.1. The program allows to observe the change of the slow variable and AP in time, to save images of the AP and slow variable distribution at any moment in time, and to continuously store the values of AP and the slow variable at some locations during the simulation. If necessary, the results of simulation (including images) can be recorded and replayed later at faster speed. The program provides the interactive mode of simulation and can be interrupted at any time in order to change parameters or regimes of simulation.

## 6.5 Measurement of the Wave Propagation Speed

It is important to know the speed of the wave front when studying the wave propagation. Since a wave can propagate in any direction, and different parts of the wave front have, in general, different speeds, we have to compute the speed for every point in space. To calculate speed, we record the time of the wave front appearance for every grid point. The wave front appearance in the certain point $i$ is detected when the following conditions are satisfied:

$$\begin{cases} \frac{dE(t_i)}{dt_i} > 0 \\ E(t_{i-1}) \leq E_{front} \\ E(t_i) > E_{front} \end{cases} \tag{6.9}$$

where $E_{front}$ is some reference point above the threshold potential. If conditions are true, $t_i$ is recorded as a time of the wave front appearance at the $i$-th point.

Consider a wave front passing through the grid points 1, 2 and 3 at times $t_1$, $t_2$ and $t_3$ (see Fig. 6.2). We can consider the wave front to be linear in the vicinity of one grid cell. Let us pick a point on the wave front. As the wave front moves with the velocity $\Theta$, this point will visit locations $A$, $B$ and $C$ at times $t_1$, $t_2$ and $t_3$. So, $\Theta$ can be found as

$$\Theta = \frac{|AB|}{t_2 - t_1} = \frac{hcos\alpha}{t_2 - t_1} \quad or \quad \Theta = \frac{|AC|}{t_3 - t_1} = \frac{hsin\alpha}{t_3 - t_1} \tag{6.10}$$

Here $\alpha = arctg\frac{t_3 - t_1}{t_2 - t_1}$ and we can compute the value of speed using either of the above formulas (6.10). To provide higher accuracy and avoid division by zero, the expression with the greater denominator is used for each particular node. The $x$-

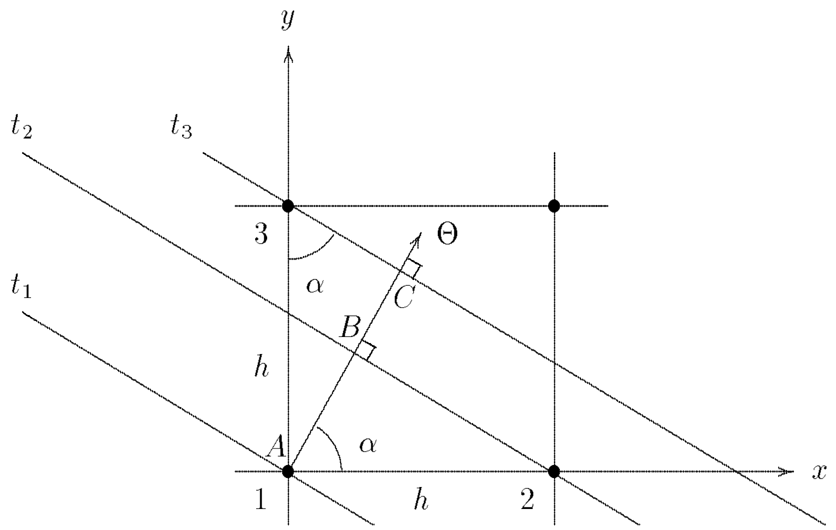


Figure 6.2: The determination of the wave front velocity.

and $y$-projections of the wave front velocity vector can be found as:

$$\Theta_x = \Theta cos\alpha \;\; ; \;\; \Theta_y = \Theta sin\alpha \tag{6.11}$$

## 6.6 Spiral Wave Propagation and Breakup

It is of special interest to study the spiral wave formation and breakup using the third-order model. The importance of this investigation is connected with the fact that spiral wave can be considered a prototype of the stationary arrhythmia and the spontaneous breakup of the non-stationary spiral wave is considered as a possible prototype of heart fibrillation.

Let us consider a square sheet of tissue with the size $200 \times 200$ nodes ($8 \times 8cm$). In the following pictures the node (1,1) is located in the upper left corner of the

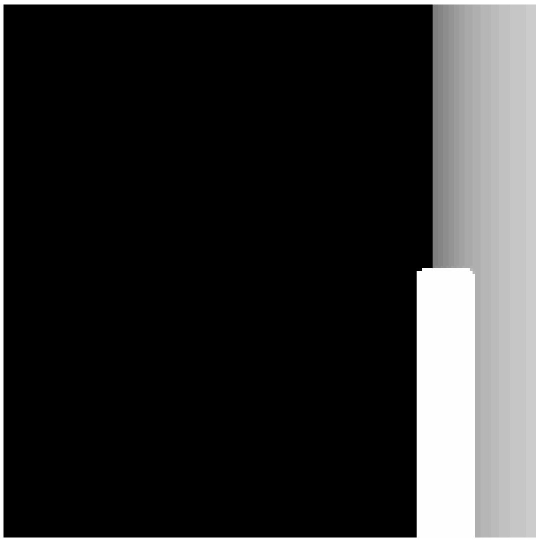

Figure 6.3: The premature beat is applied too close to the wave. Stimulus at ((155,100), (175,200)). Wave tail at 160.

Figure 6.4: The premature beat is applied too close to the wave. Propagation fails.

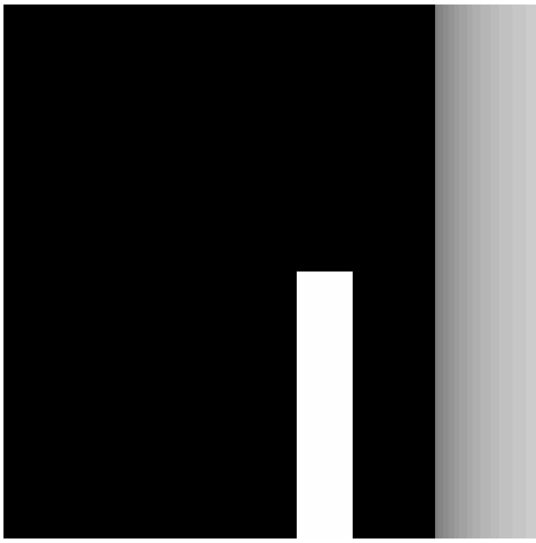

Figure 6.5: The premature beat is applied too far from the wave. Stimulus at ((110,100), (130,200)). Wave tail at 160.

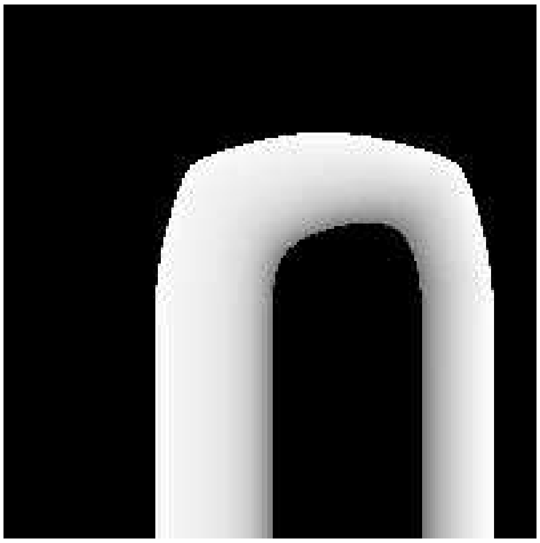

Figure 6.6: The premature beat is applied too far from the wave. The spiral wave doesn't appear.

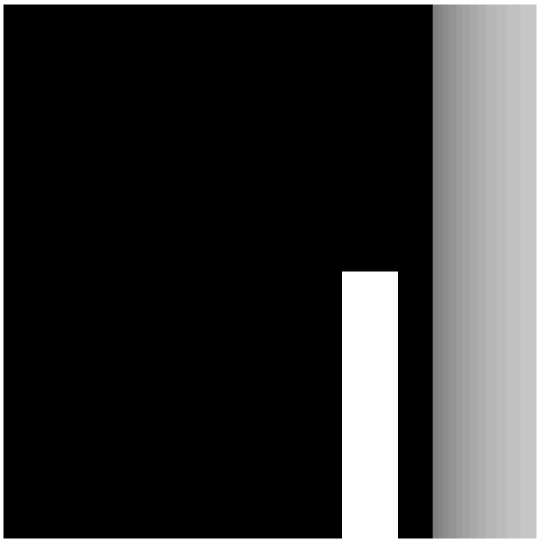

Figure 6.7: The premature beat is applied at ((127,100), (147,200)). Wave tail at 160. $t = 0ms$.

grid. We initiate the spiral wave propagation by applying the premature beat on the tail of the rectilinear wave. The appearance of the spiral wave depends upon the position of the premature beat relative to the wave tail. If the beat is applied too close to the wave (Fig. 6.3), the propagation of the newborn wave fails (Fig. 6.4). If the beat is applied too far from the wave (Fig. 6.5) the semi-circular wave appears and, then, disappears reaching the boundary of the tissue (Fig. 6.6). To produce a spiral wave, we applied the premature beat as shown in Fig. 6.7. The dimensions of the premature beat are 20 nodes by 100 nodes. The stimulus was applied at the distance 13 nodes from the point on the tail where AP is 90% of $|E_{max}|$. The stimulus was applied for 1.5 $ms$ with the amplitude $-40\mu A/cm^2$.

The simulation results were obtained using the APD restitution described in section 5.5 for the following values of the tissue parameters: $\Delta t = 0.03ms$,

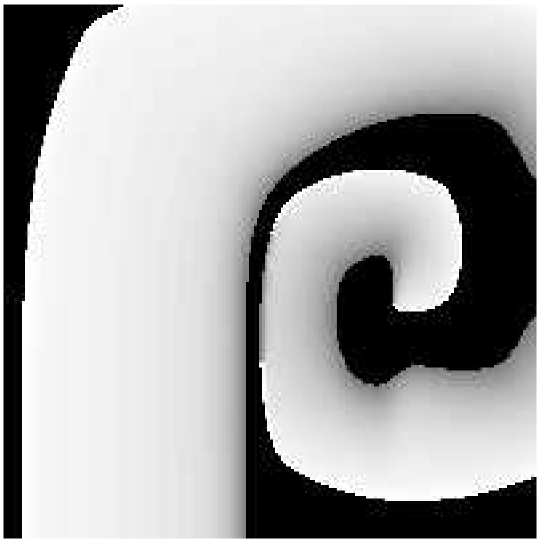

Figure 6.8: The wave is about to break. $t = 109.5ms$.

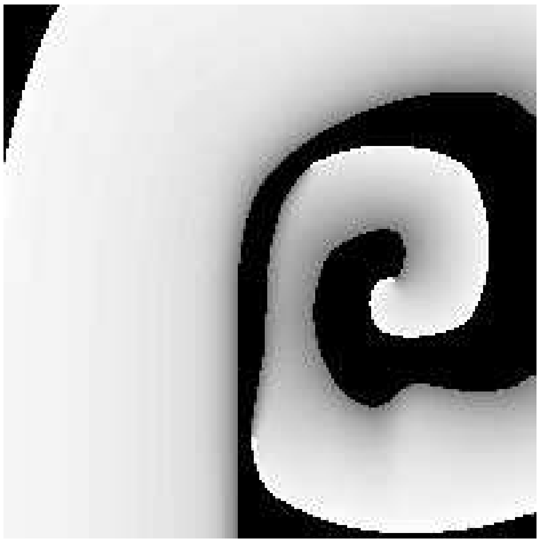

Figure 6.9: The wave after the first break. $t = 120.0ms$.

Figure 6.10: The wave splits into two parts. $t = 127.5ms$.

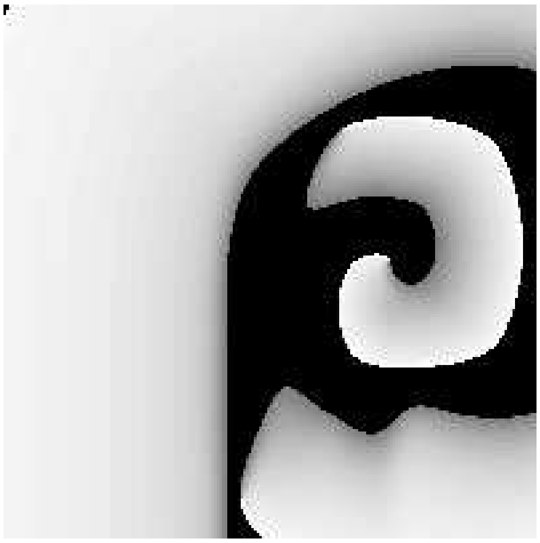

Figure 6.11: After the breakup, each part of the wave becomes an independent spiral. $t = 133.5ms$.

Figure 6.12: The second breakup of the wave. $t = 190ms$.

$\Delta h = 0.04cm$, diffusion coefficient 0.0012 $m\Omega^{-1}$, tissue size $200 \times 200$ nodes. The velocity of the rectilinear front propagation was 37 $cm/s$.

With these parameters, the initiated spiral wave is non-stationary and it starts to break on the second turn when, at some point, the front of the wave comes too close to the tail (Fig. 6.8). This causes the front to slow down up to the point when further propagation stops. The rest of the front, however, continues to propagate (Fig. 6.9). As a result, the wave splits into two parts (Fig. 6.10), each of which becomes an independent spiral (Fig. 6.11). This process repeats (Fig. 6.12), so, finally, we obtain a number of spirals rotating in different directions (Fig. 6.13). The structure of rotating spirals changes all the time due to their meandering (Fig. 6.14). For smaller tissue size ($128 \times 128$ nodes), it was observed that these spiral waves move off the tissue area after some time. The same effect was observed by Karma [Kar93]. For the tissue size $200 \times 200$ nodes, however, this doesn't occur. The APD recording in a cell located in the middle of the

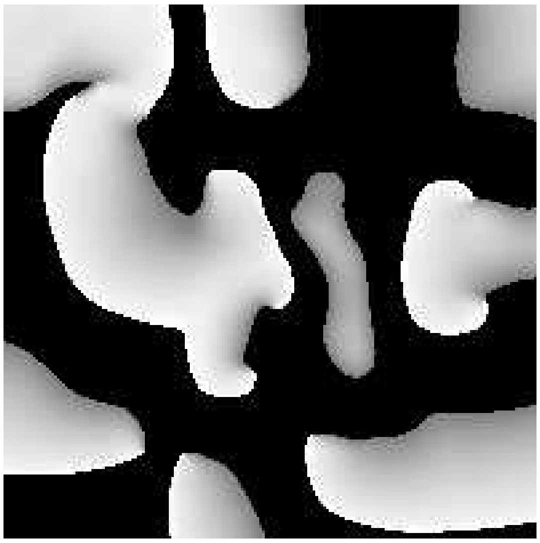

Figure 6.13: The spirals rotating in different directions. $t = 8998.5ms$.

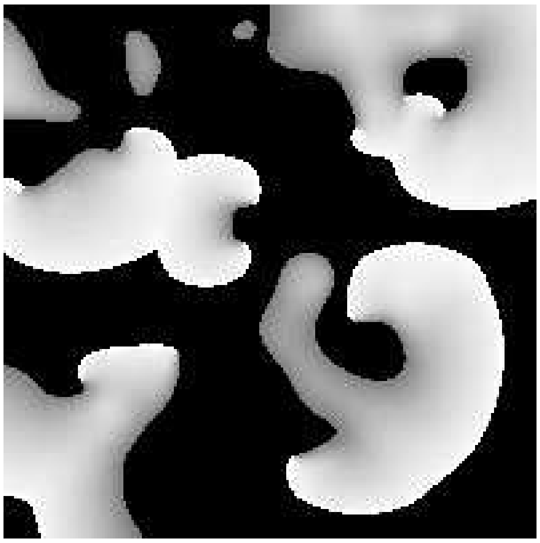

Figure 6.14: The changing structure of spirals. $t = 9298.5ms$.

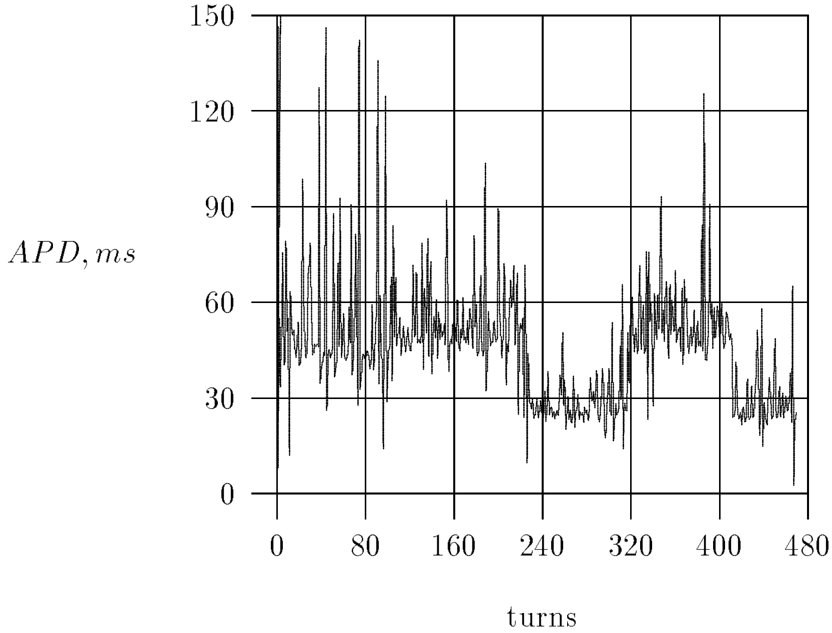


Figure 6.15: APD recordings in the middle of the simulated tissue.

simulated tissue presented in Fig. 6.15. It is not structured in any way, which hints to the irregular behavior of the spirals.

In order to find the effect of the $(dE/dt)_{max}$ restitution on the wave propagation in 2D tissue the presented experiments were repeated with the modified gate variable $j$ as it was done in chapter 5 (see (5.6)). This modification eliminates the $(dE/dt)_{max}$ restitution. Fig. 6.16 – 6.20 show the distribution of spiral waves in successive intervals of time. One can notice that in the case with modified $j$ the image structure repeats periodically, while in the case with the original $j$ ($(dE/dt)_{max}$ restitution present) the structure of spirals changes irregularly. In the experiment with the Karma model [Kar93], which doesn't take into consideration $(dE/dt)_{max}$ restitution, the regular structure of multiple spiral waves also was observed.

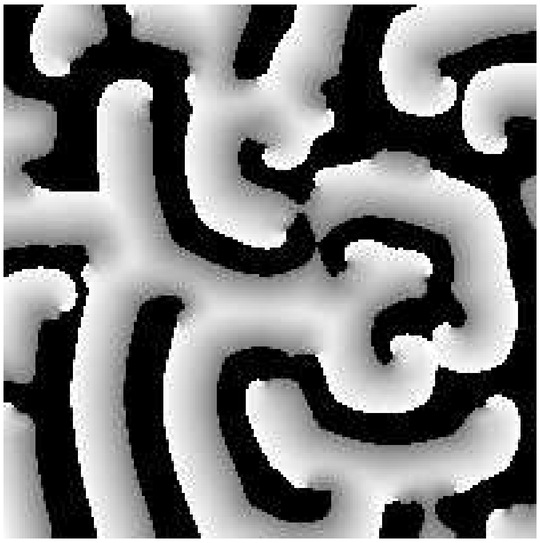

Figure 6.16: The spiral rotation without $j$. $t = 8998.5ms$.

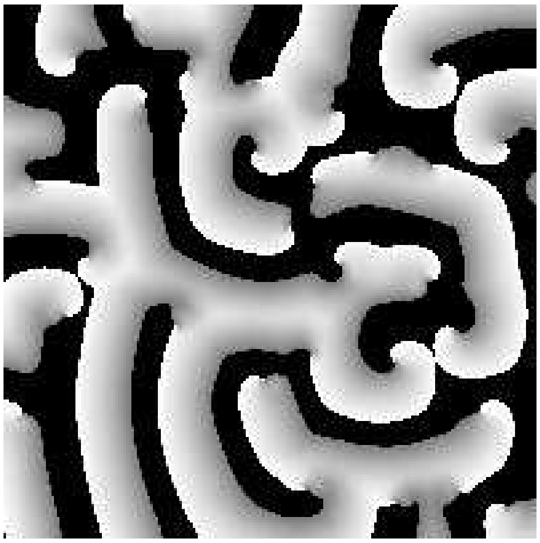

Figure 6.17: The spiral rotation without $j$. $t = 9027ms$.

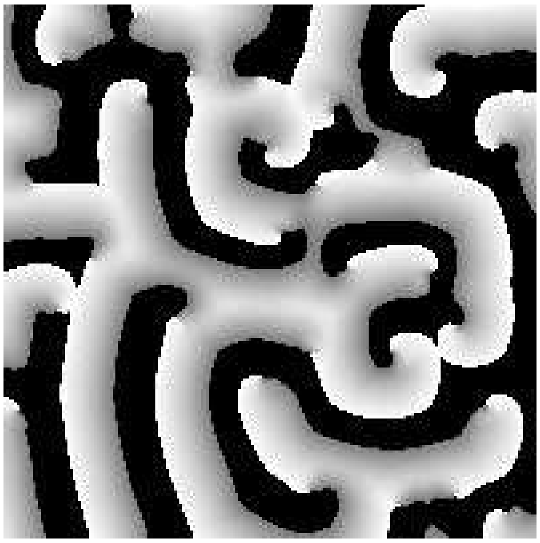

Figure 6.18: The spiral rotation without $j$. $t = 9742.5ms$.

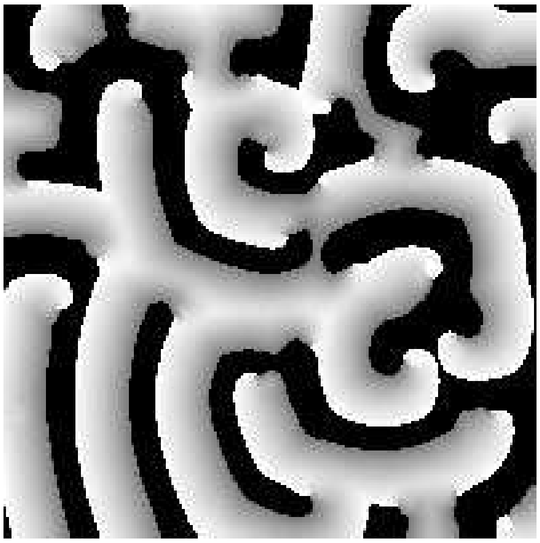

Figure 6.19: The spiral rotation without $j$. $t = 10488ms$.

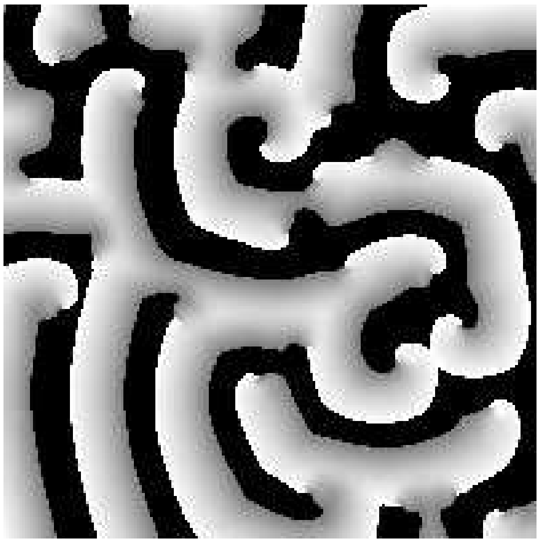

Figure 6.20: The spiral rotation without $j$. $t = 10600.5ms$.

## 6.7 Conclusion

1. The third-order simplified model with an $S$-shaped static APD restitution curve, which has slope greater than 1, allows to obtain the breakup of the non-stationary spiral wave initiated by the premature beat.

2. The $(dE/dt)_{max}$ restitution plays an important role in 2D propagation. With the presence of the $(dE/dt)_{max}$ restitution the multiple spiral waves propagate irregularly. Without $(dE/dt)_{max}$ restitution the multiple spiral waves form stable structure after some transient period of time.

3. There is a critical size of the 2D grid of cells which provides long-term existence of irregular multiple spiral waves.

4. There exists in space a window of vulnerability where the application of the premature beat causes the appearance of a non-stationary spiral wave.

5. The method is proposed to determine the wave front propagation velocity based on the measurement of time of the wave front arrival to the neighboring cells of the grid.

# CHAPTER 7

# Conclusion

## 7.1 Objectives

Computer simulation is a well recognized tool for the investigation of various dynamic processes. For the last 20 – 25 years computer simulation has been widely used for the investigation of the electrophysiological processes in the heart, especially heart fibrillation, which is recognized as a main cause of sudden cardiac death. In spite of the tremendous progress in computer technology during recent years, until now it was impossible to get quantitative results, especially for 2D and 3D cardiac tissue. The great complexity of the cardiac cell mathematical model derived from the clamp experiments doesn't allow us to simulate 2D and 3D AP propagation in reasonable time. The existing simplified models give only qualitative estimates of the propagation character. The creation of a simplified model which retains all of the necessary characteristics for the simulation of the propagation phenomena is a challenging task.

The goal of this research effort has been to develop and evaluate such a simplified model of cardiac AP which will be valid for studying propagation in normal and abnormal tissue.

The objective of the research was to show:

- How to synthesize the simplified model on the base of a given full physiological model.

- The properties of the existing simplified models, underlining their advantages and disadvantages.
- The importance of the $(dE/dt)_{max}$ restitution in the AP propagation model.
- The effect of APD and $(dE/dt)_{max}$ restitutions on 1D and 2D AP propagation.
- That for this kind of problem the tabulation of non-linear functions can provide significant computational speed up.

## 7.2 Summary

In an effort to answer the primary research questions, this thesis covered the following topics:

1. **Theoretical analysis and comparison of the existing simplified models.** This included the development of a common approach to the analysis of the various simplified models.
2. **The development of a third-order simplified model.** The third-order simplified model was constructed on the base of the LR I model. For this purpose, the new functions for the currents participating in the depolarization and repolarization phases were constructed and implemented in tables. The method of adjusting the model for the required APD restitution curve was developed.

3. **Investigation of AP propagation in a ring of cells.** The AP propagation in the ring was studied for different APD restitution curves and compared with the LR model.

4. **Investigation of AP propagation in the 2D uniform tissue.** The propagation in the $8 \times 8cm$ sheet of cardiac tissue was simulated using the simplified third-order model. The conditions for the origination of the spiral wave and its breakup were studied.

## 7.3 Computer Science Issues

In addition to the analysis and synthesis of the cardiac models, the following issues were addressed to provide effective and convenient programming tools for simulations:

- **The choice and analysis of the numerical algorithms.** The Ashour–Hanna numerical algorithm for integration of the stiff ODE was chosen, and its parameter $\alpha$ was optimized to obtain the maximum time step of integration providing required accuracy and stability.

- **Accuracy of long simulations.** To avoid the accumulation of round off errors during long term simulations, the computation of the simulation time was done through counting the number of integration steps.

- **Automatic table generation for non-linear functions.** To speed up computation the simplified model uses tables for non-linear function representation. A method of automatic table generation was developed.

- **Using tabular representation of APD restitution.** The APD restitution table is automatically generated from the given APD restitution curve using developed fitting algorithm. This method allows us to implement any restitution curve for a given model.

- **Measurement of AP parameters.** The algorithms for automatic measurement of AP parameters and AP propagation velocity were developed.

- **Interactive user interface and graphics.** The interactive user interface for the simulation program was developed, which allows intervention into the simulation process. The graphical output of the simulation results for 1D and 2D models was developed using X-windows. As an option, the mechanism for saving the simulation results for future replay was provided.

## 7.4 Contributions

In this research effort, a third-order simplified mathematical model of cardiac cell was developed. This model retains all properties of the LR I model important for AP propagation, but at the same time is much faster for simulation than the full physiological model, thus opening a new avenue to realistic 3D propagation simulation. This model has been validated for 1D and 2D propagation and has allowed to obtain new important results and findings.

The scientific and engineering contributions of this work include the following:

1. **The comparative analysis of the existing simplified models realized using proposed $I$–$E$ phase plane** showed that all of the simplified models are based on the same assumptions and differ in analytical approximations of experimental dependencies of $I_{inw}(E)$ and $I_{outw}(E)$ and in the

way the slow variable affects the outward current. They all produce decreased $(dE/dt)_{max}$ and do not correctly reproduce the APD restitution properties.

2. **The method of synthesis of the third-order simplified model of cardiac cell is developed.** It is based on the separation of the all membrane currents of the full model into two groups: currents participating in the depolarization phase and currents participating in the repolarization phase. This method allows us to construct the third-order model for any modern physiological model, which correctly reproduces the recovery properties of the cell.

3. In the generation of one AP the use of the third-order simplified model (based on the LR model) with the tabulated non-linear functions gives a **95 % decrease of computation time** in comparison with the LR I full model, and about a 35 % decrease in comparison with the VC-D second-order model.

4. **The method of implementing the given restitution curve in the simplified model** by introducing the coefficient for the repolarization current and using automatic table generation.

5. **New phenomena were discovered during 1D AP propagation**:

   - $(dE/dt)_{max}$ restitution increases the range of ring lengths where the instability can be observed;
   - the single cell APD restitution curve is significantly changed for the cell placed in the ring during quasi-periodic instability – it is double-valued and shifted with respect to the static ADP restitution curve;

- the shape and the slope of the static APD restitution curve determines the region of ring lengths corresponding to quasi-periodic instability;
- during quasi-periodic instability the APD distribution along the ring is periodic with the period $\lambda$, which is less than two ring lengths as it was shown theoretically;
- the period of slow modulated oscillations can be determined as $T = 2L/(2L - \lambda)$.

6. **New phenomena were discovered during 2D AP propagation**:
   - the breakup of the non-stationary spiral wave initiated by the premature beat in tissue with an $S$-shaped static APD restitution curve;
   - this breakup differs from the one obtained using other simplified models due to the effect of $(dE/dt)_{max}$ restitution, which leads to the irregularity of the structure of the obtained spiral waves.

## 7.5 Suggestions for Future Research

Following is a broad description of some of the research that needs to be done in this field.

**2D simulations.** Since spiral electrical activity in the heart tissue is considered a cause of heart arrhythmia, more research is needed to:

- determine the conditions which prevent spiral wave breakup and spiral wave propagation;
- find some general criteria that will show the presence of spiral waves in the tissue;

- find ways to prevent further propagation of existing spiral waves and their breakup.

**3D simulations.** The simulation of AP propagation in 3D cardiac tissue using the proposed model is the next step in this research. In this respect, it is important to compare the results obtained for the spiral wave breakup in 2D simulation with the spontaneous scroll wave breakup in the 3D case. The verification of the 3D simulations will require new physiological experiments, since no 3D physiological data are available today.

**New heart simulation methodology.** The development of a new approach in which cardiac tissue is represented as a bunch of heart muscle fibers promises to open a new avenue in the investigation of wave propagation in the heart. The new methodology is particularly important in the simulation of wave propagation using the real geometry of the heart. Today, the detailed geometry of the heart is studied, including the dynamic changes during the heartbeat. To combinate the AP generation model with a model reflecting the dynamic geometry of the heart would represent a real challenge in this field.

# References


[AH90] S.S. Ashour and O.T. Hanna. "A New very Simple Explicit Method for the Integration of Mildly Stiff Ordinary Differential Equations." *Computers chem. Engng*, **14**(3):267–272, 1990.

[Bon59] K. Bonhoeffer. In *Proceedings of 4th Electrochemistry Conference*, Moscow, 1959. Izdat. Akad. Nauk SSSR.

[BR77] G.W. Beeler and H. Reuter. "Reconstruction of the action potential of ventricular myocardial fibers." *J. Physiol.*, **268**:177–210, 1977.

[CGK93] Marc Courtemanche, Leon Glass, and James P. Keener. "Instabilities of a Propagating Pulse in a Ring of Excitable Media." *Physical Review Letters*, **70**(14):2182–2185, 1993.

[DN85] D. DiFrancesco and D. Noble. "A model of cardiac electrical activity incorporating ionic pumps and concentration changes." *Phil. Trans. R. Soc. London Ser. B*, **307**:353–398, 1985.

[EJ80] L. Ebihara and E.A. Johnson. "Fast sodium current in cardiac muscle: A quantitative description." *Biophys. J.*, **32**:779–790, 1980.

[EPS89] E.A. Ermakova, A.M. Pertsov, and E.E. Shnol. "On the interaction of vortices in two-dimensional active media." *Physica D*, **40**:185–195, 1989.

[Fit69] R. FitzHugh. "Mathematical models of excitation and propagation in nerve." In H.P. Schwan, editor, *Biological Engineering*, chapter 1, pp. 1–85. McGraw-Hill, New York, 1969.

[FS88] Lawrence H. Frame, MD and Michael B. Simson, MD. "Oscillations of Conduction, Action Potential Duration, and Refractoriness. A Mechanism for Spontaneous Termination of Reentrant Tachycardias." *Circulation*, **78**(5):1277–1287, 1988.

[GKR67] F.B. Gulko, B.Y. Kogan, and M.E. Rajskina. "On possible application of computers for studying the mechanisms of diseases." *Automation and Remote Control*, **8**, 1967.

[GP70] F.B. Gulko and A.A. Petrov. "On a mathematical model of excitation processes in Purkinje fiber." *Biofizika*, **15**:513–520, 1970.

[GP72] F.B. Gulko and A.A. Petrov. "Mechanism of the formation of closed pathways of conduction in excitable media." *Biofizika*, **17**:271–282, 1972.

[GT60] I.M. Gelfand and M.L. Tsetlin. "On continual models of control systems." *DAN SSSR*, **131**(6), 1960.

[HH52] A.L. Hodgkin and A.F. Huxley. "A quantitative description of membrane current and its application to conduction and excitation in nerve." *J. Physiol.*, **117**:500, 1952.

[Hoy68] R.C. Hoyt. "Sodium Inactivation in Nerve Fibers." *Biophys. J.*, **8**:1074–1094, 1968.

[IKS78] G.R. Ivanitsky, V.I. Krinsky, and I.I. Selkov. *Mathematical biophysics of the cell.* Nauka, Moscow, 1978.

[Kar93] A. Karma. "Spiral Breakup in Model Equations of Action Potential Propagation in Cardiac Tissue." *Physical Review Letters*, **71**(7):1103–1106, 1993.

[Kar94] A. Karma. "Electrical Alternans and Spiral Wave Breakup in Cardiac Tissue." *Chaos*, **4**(3), 1994.

[KK73] V.I. Krinsky and Yu. M. Kokoz. "Analysis of equations of excitable membranes. III. The membrane of the Purkinje fiber." *Biofizika*, **18**(6), 1973.

[KKB91a] B.Y. Kogan, W.J. Karplus, B.S. Billett, and M.G. Karpoukhin. "On the applicability of the Ashour – Hanna numerical algorithm for the investigation of reaction–diffusion equations." Technical Report 910076, Computer Science Department, UCLA, November 1991.

[KKB91b] B.Y. Kogan, W.J. Karplus, B.S. Billett, A.T. Pang, H.S. Karagueuzian, and S.S. Khan. "The Simplified FitzHugh-Nagumo Model With Action Potential Duration Restitution: Effects on 2D Wave Propagation." *Physica D*, **50**:327–340, 1991.

[KKB93] B.Y. Kogan, W.J. Karplus, B.S. Billett, and M.G. Karpoukhin. "Excitation Wave Front Transients: A Computer Simulation Study." In *Proceedings of the 15th Annual International Conference of the IEEE Engineering In Medicine and Biology Society*, pp. 28–31, San Diego, CA, October 1993.

[KKK95a] Mikhail G. Karpoukhin, Boris Y. Kogan, and Walter J. Karplus. "The Application of a Massively Parallel Computer to the Simulation of Electrical Wave Propagation Phenomena in the Heart Muscle Using Simplified Models." In *Proceedings of the Twenty-Eighth Annual Hawaii International Conference on System Sciences. Biotechnology Computing*, volume 5, pp. 112–122. IEEE Computer Society Press, 1995.

[KKK95b] B.Y. Kogan, W.J. Karplus, and M.G. Karpoukhin. "The Third-Order Action Potential Model for Computer Simulation of Electrical Wave Propagation in Cardiac Tissue." In H. Power and R.T. Hart, editors, *Computer Simulations in Biomedicine*. Computational Mechanics Publications, Southampton Boston, 1995.

[KKK96] Boris Y. Kogan, Walter J. Karplus, and Mikhail G. Karpoukhin. "The Van Capelle and Durrer Model of Cardiac Action Potential Generation and 2D Propagation: Modifications and Application to Spiral Wave Propagation." In James G. Anderson and Meyer Katzper, editors, *Simulation in the Medical Sciences conference. Proceedings of the 1996 Western Multiconference*, pp. 106–112. The Society for Computer Simulation, January 1996.

[KLZ94] A. Karma, H. Levine, and X. Zou. "Theory of Pulse Instabilities in Electrophysiological Models of Excitable Tissues." *Physica D*, **73**:113–127, 1994.

[Kri71] V.I. Krinsky. "Nonstationary velocity of excitation propagation, latent periods and their relationship with heart fibrillation." *Biofizika*, **16**(1), 1971.

[LGR94] Kenneth R. Laurita, MS, Steven D. Girouard, MS, and David S. Rosenbaum, MD. "Arrhythmogenic Preconditioning by Single Premature Stimuli." *PACE*, **17**:762, 1994.

[LR91] C. Luo and Y. Rudy. "A Model of the Ventricular Cardiac Action Potential." *Circ. Res.*, **68**:1501–1526, 1991.

[LR94] C. Luo and Y. Rudy. "A Dynamic Model of the Cardiac Ventricular Action Potential." *Circ. Res.*, **74**(6):1071–1113, 1994.

[MNT75] R.E. McAllister, D. Noble, and R.W. Tsien. "Reconstruction of the electrical activity of cardiac Purkinje fibers." *J. Physiol.*, **251**:1–59, 1975.

[MRA64] G.K. Moe, W.C. Rheinboldt, and J.A. Abildskov. "A computer model for atrial fibrillation." *Amer. Heart. J.*, **67**:200–220, 1964.

[NAY62] J. Nagumo, S. Arimoto, and S. Yoshizava. "An active pulse transmission line simulating nerve axon." *Proc. IRE*, **50**:2061, 1962.

[Nob62] D. Noble. "A modification of the Hodgkin - Huxley equations applicable to Purkinje fiber action and pace-maker potentials." *J. Physiol.*, **160**:317–352, 1962.

[NW87] P.I. Nadapurkar and A.T. Winfree. "A computation study of twisted linked scroll waves in excitable media." *Physica D*, **29**:69–83, 1987.

[Ost00] W. Ostwald. *Ztschr. Phys. Chem.*, **37**:33–42, 1900.

[PCP81] A.M. Pertsov, R.N. Chramov, and A.V. Panfilov. "Sharp increase in refractory period induced by oxidation suppression in FitzHugh-Nagumo model. New mechanism of anti-arrhythmic drug action." *Biofizika*, **6**, 1981. (in Russian).

[PDS93] Arkady M. Pertsov, Jorge M. Davidenko, Remy Salomonsz, William T. Baxter, and Jose Jalife. "Spiral Waves of Excitation Underlie Reentrant Activity in Isolated Cardiac Muscle." *Circ. Res.*, **72**(3):631–650, 1993.

[PEP84] A.M. Pertsov, E.A. Ermakova, and A.V. Panfilov. "Rotating spiral waves in a modified FitzHugh-Nagumo model." *Physica D*, **14**:117–124, 1984.

[Pet75] A.A. Petrov. "Hybrid method of solving partial differential equations." *Avtom. Telemeka.*, **3**, 1975.

[PP81] A.M. Pertsov and A.V. Panfilov. "Spiral waves in active media. Reverberator in FitzHugh-Nagumo model." In *Autowave processes in systems with diffusion*, pp. 77–89. Institute of Applied Physics Academy of Science USSR, 1981. (in Russian).

[SSZ88] M.C. Sanguinetti, A.L. Scott, G.J. Zingaro, and P.K. Siegl. "BRL 34915 (cromakalim) activates the ATP-sensitive K current in cardiac muscle." *PNAS*, **85**:8360–8364, 1988.

[Tik52] A.N. Tikhonov. "Differential equations with small parameters at derivatives." *Mathematical collection*, **31(73)**(3), 1952.

[TK88] J.J. Tyson and J.P. Keener. "Singular Perturbation Theory of Traveling Waves in Excitable Media." *Physica D*, **32**:327–361, 1988.

[VD80] Frans J. L. Van Capelle and Dirk Durrer. "Computer Simulation of Arrhythmias in a Network of Coupled Excitable Elements." *Circ. Res.*, **47**(3):454–466, 1980.

[VV28] B. Van der Pol and J. Van der Mark. "The heartbeat considered as a relaxation oscillation, and an electrical model of the heart." *Philos. Mag. Suppl.*, **6**:763–775, 1928.

[Win87] A.T. Winfree. *When Time Breaks Down.* Princeton University Press, Princeton, New Jersey, 1987.

[Win89] A.T. Winfree. "Electrical instability in cardiac muscle: Phase singularities and rotors." *J. Theor. Biol.*, pp. 353–405, 1989.

[WR46] N. Wiener and A. Rosenblueth. "The mathematical formulation of the problem of conduction of impulses in a network of connected excitable elements, specifically in cardiac muscle." *Arch. Inst. Cardiologia de Mexico*, **16**(3), 1946.

[Zyk87] V.S. Zykov. *Simulation of Wave Processes in Excitable Media.* Manchester University Press, 1987.